Doctor's Thesis

Green synthesis of nanoparticles and their applications to bio-environmental fields

Vemu Anil Kumar

4R10130001

3rd Year

Doctor Course
Course of Bio-Nano Science Fusion
Graduate School of Interdisciplinary New Sciences
Toyo University, Japan

Academic Year's 2016

Preface

The present research is focused on the Green methodology to synthesise nanoparticles by using aqueous leaf extracts to application in bio-environmental fields. In chapter 2, *Prunus yedoensis* leaf extract was used to synthesise biocompatible silver nanoparticles. It is the fact; much leaf extracts posses' supreme medicinal properties, where even raw leaf extracts are used to treat various dreadful infections and diseases. The prime motive of the work is to utilise the properties of *Prunus yedoensis* leaf extract to synthesise silver nano particles which holds medicinal properties and more over biocompatible, so that both the properties of silver nanoparticles and leaf extract can be utilised together in synthesising novel nanoparticles that can be used as a Nano medicine. In chapter 3, leaf extract of a weed species *Solidago altissima* was used to synthesise nanoparticles composed of silver and silver chloride which is a plasmonic photo catalyst; *Solidago altissima* is considered to be a potential threat for wetlands that cause economic damage to the agriculture fields in Japan. The leaf extract of the weed species consists of abundant chlorine components, which lead to synthesise silver chloride nanoparticles. In chapter 4, nanoparticles composed of silver and silver chloride were synthesised based on the methodology of chapter 3. The intention to support Japan economy as mentioned by the MEXT- Japan, with scientific knowledge is partially fulfilled by the present work, however an immense further research is to be proceeded.

This thesis is submitted for the degree of Doctor of Philosophy at the Toyo University, Kawagoe, Japan. The research done, to the best of my knowledge is original except the references mentioned. Neither this nor similar thesis of this work has been submitted for any other purposes.

Vemu Anil Kumar

CONTENTS

Introduction

The research focused on the phyto synthesis of nanoparticles by bio-reduction of metal salt solution with aqueous leaf extract of different plants. The work proceeded aiming at proper utilisation of aqueous leaf extracts and metal salts in synthesising nanoparticles, to bring the cost of synthesis as low as possible and to make the synthetic procedures as simple as possible following ambient conditions. At a maximum effort, toxic chemicals and complicated experimental protocols were avoided, even though better results were put forth in both synthesis and applications. A wide range of characterisation was executed to determine properties of the pristine nanoparticles, so that as-synthesised particles were used in various fields.

Metal nanoparticles (MNPs) are much significant in science and technology because of their extraordinary beneficial physical, chemical and biological properties to develop and engineer sophisticated modish products not only limited to research but also at commercial scale. Notable properties of MNPs are mainly due to high surface area to volume ratio and other properties like specific optical properties, mechanical strengths, lower melting points and specific magnetizations, which promote their applications in various fields. The intrinsic properties of MNPs are mainly determined by its size, shape, composition, crystallinity, surface functionality and solid / hollow structure which differs from bulk metals. In fact, these parameters can be controlled to fine-tune the properties. MNPs include pure metal nanoparticles, metal-oxide nanoparticles, alloy nanoparticles and composite nanoparticles coupled with some other non-metallic compounds. Among MNPs Silver nanoparticles (Ag NPs) are extensively studied for decades due to their unique surface plasmon resonance properties in visible region. [1]

Nano silver have 120 years of history.[2] Ag NPs are in significant demand at not only a research level, but also even a commercial one worldwide thanks to their distinctive physicochemical properties such as high electrical and thermal conductivities, surface enhanced Raman scattering ability, chemical stability, catalytic activity and nonlinear optical behavior [3]. Ag NPs have been extensively used in the fields of medicine, physics, materials science, chemistry

[4] [5] and agriculture. [6] They have been actively utilized particularly in electronics, photonics, chemical sensing/imaging, drug delivery/bio-labeling, [7, 8] textile industry, food industry,[6] degradation of organic pollutants and water purification[9]. Ag NPs have also been used in recent years as an antimicrobial agent to prevent infections and have also found many uses in medical products, such as antibacterial surface coatings of stents, breathing tubes, heart valves, catheters, surgical masks, and wound dressings.[10, 11]. Ag NPs based consumer products extensive usage can be seen in personal care and cosmetics, textiles, electronics, household products/home improvement, and filtration/purification/sanitization devices.[12]. All together the applications of Ag NPs can be generally categorized under three, such as consumer goods, biomedicine and food production and packing. Project on Emerging Nanotechnologies (PEN) have stated the statistical data of utilization of Ag NPs in this generation.[13]

Synthesis of Ag NPs can be proceeded by physical, chemical and biological methods,[14] [15]but biological syntheses are advantageous in such a sense that it is cost effective and environmentally friendly, and furthermore there is no need for high pressure, high temperature and toxic chemicals[16]. So Synthesis of metal nanoparticles by green protocols is of great demand[17]. Integration of green chemistry in the synthesis of nanomaterials promotes both performance and safety[18]. In the biological synthetic methods, either microorganisms[19, 20] or plant extracts[21-23]are commonly used. It is supposed that using plants for synthesis of Ag NPs may be quite reasonable even compared to the other biological methods since several elaborate processes such as cell culture maintenance and specific handling procedures under aseptic conditions can be eliminated[24].

On the other hand Ag NPs when associated with other materials forms nano-composite materials that promotes applications in various fields based on their distinctive properties. In recent years Ag@AgCl nanoparticles drawn many researchers of its photo catalytic activity in visible light. Ag@AgCl NPs are acknowledged to be an efficient and stable photo catalyst under irradiation of visible light [25-29]. Silver nanoparticles (Ag NPs), which are one of the noble

metal ones due to surface plasmon resonance (SPR) effect, have a strong visible light absorption ability [30]; whereas Silver chloride nanoparticles (AgCl NPs), which posses promising electronic, magnetic, optical and catalytic properties [31]; act as photosensitive semiconductor with a direct bandgap of 5.15 eV (241 nm) and indirect bandgap of 3.25 eV (382 nm)[32] [33]. Nanoparticles composed of both Ag with AgCl (Ag@AgCl NPs) would therefore act as an efficient plasmonic visible light photo catalyst[34, 35]. Photo catalyst in general synthesised by hydrothermal method [36], *in-situ* anion exchange method [37] and *in-situ* photoactive method [38]. So there is a need to develop green methods to synthesise such nanoparticles.

References

1. M. Jakob, H. Levanon and P. V. Kamat, *Nano Letters*, 2003, **3**, 353-358.

2. B. Nowack, H. F. Krug and M. Height, *Environmental Science & Technology*, 2011, **45**, 1177-1183.

3. Y. A. Krutyakov, A. A. Kudrinskiy, A. Y. Olenin and G. V. Lisichkin, *Journal*, 2008, **77**.

4. D. R. Bhumkar, H. M. Joshi, M. Sastry and V. B. Pokharkar, *Pharmaceutical Research*, 2007, **24**, 1415-1426.

5. C. A. J. Lin, T. Y. Yang, C. H. Lee, S. H. Huang, R. A. Sperling, M. Zanella, J. K. Li, J. L. Shen, H. H. Wang, H. I. Yeh, W. J. Parak and W. H. Chang, *Acs Nano*, 2009, **3**, 395-401.

6. R. Nair, S. H. Varghese, B. G. Nair, T. Maekawa, Y. Yoshida and D. S. Kumar, *Plant Science*, 2010, **179**, 154-163.

7. M. C. Daniel and D. Astruc, *Chemical Reviews*, 2004, **104**, 293-346.

8. R. Guo, Y. Song, G. L. Wang and R. W. Murray, *Journal of the American Chemical Society*, 2005, **127**, 2752-2757.

9. N. Durán, P. D. Marcato, O. L. Alves, G. I. D. Souza and E. Esposito, *Journal of Nanobiotechnology*, 2005, **3**, 1-7.

10. U. Samuel and J. P. Guggenbichler, *International Journal of Antimicrobial Agents*, 2004, **23**, S75-S78.

11. Y. Li, P. Leung, L. Yao, Q. W. Song and E. Newton, *Journal of Hospital Infection*, 2006, **62**, 58-63.

12. S. W. P. Wijnhoven, W. Peijnenburg, C. A. Herberts, W. I. Hagens, A. G. Oomen, E. H. W. Heugens, B. Roszek, J. Bisschops, I. Gosens, D. Van de Meent, S. Dekkers, W. H. De Jong, M. Van Zijverden, A. Sips and R. E. Geertsma, *Nanotoxicology*, 2009, **3**, 109-U178.

13. T. Quang Huy, N. Van Quy and L. Anh-Tuan, *Advances in Natural Sciences: Nanoscience & Nanotechnology*, 2013, **4**, 033001 (033020 pp.)-033001 (033020 pp.).

14. H. C. Chen, M. C. Roco, X. Li and Y. L. Lin, *Nature Nanotechnology*, 2008, **3**, 123-125.

15. K. M. M. Abou El-Nour, A. Eftaiha, A. Al-Warthan and R. A. A. Ammar, *Arabian Journal of Chemistry*, 2010, **3**, 135-140.

16. C. N. Lok, C. M. Ho, R. Chen, Q. Y. He, W. Y. Yu, H. Sun, P. K. H. Tam, J. F. Chiu and C. M. Che, *Journal of Biological Inorganic Chemistry*, 2007, **12**, 527-534.

17. S. Iravani, *Green Chemistry*, 2011, **13**, 2638-2650.

18. M. J. Mulvihill, E. S. Beach, J. B. Zimmerman and P. T. Anastas, in *Annual Review of Environment and Resources, Vol 36*, eds. A. Gadgil and D. M. Liverman, Annual Reviews, Palo Alto, 2011, vol. 36, pp. 271-293.

19. D. Mandal, M. E. Bolander, D. Mukhopadhyay, G. Sarkar and P. Mukherjee, *Applied Microbiology and Biotechnology*, 2006, **69**, 485-492.

20. K. N. Thakkar, S. S. Mhatre and R. Y. Parikh, *Nanomedicine-Nanotechnology Biology and Medicine*, 2010, **6**, 257-262.

21. A. K. Mittal, Y. Chisti and U. C. Banerjee, *Biotechnology Advances*, 2013, **31**, 346-356.

22. H. P. Borase, B. K. Salunke, R. B. Salunkhe, C. D. Patil, J. E. Hallsworth, B. S. Kim and S. V. Patil, *Applied Biochemistry and Biotechnology*, 2014, **173**, 1-29.

23. P. A. Poonam Patel, Sajjan Kanawaria, Sumita Kachhwaha, S. L. Kothari, in *Nanotechnology and Plant Sciences*, ed. M. H. A.-W. Manzer H. Siddiqui, Firoz Mohammad, Springer International Publishing, Switzerland, 2015, ch. 13, pp. 271-288.

24. S. S. Shankar, A. Rai, A. Ahmad and M. Sastry, *Journal of Colloid and Interface Science*, 2004, **275**, 496-502.

25. P. Wang, B. B. Huang, X. Y. Qin, X. Y. Zhang, Y. Dai, J. Y. Wei and M. H. Whangbo, *Angewandte Chemie-International Edition*, 2008, **47**, 7931-7933.

26. X. C. Ma, Y. Dai, L. Yu, Z. Z. Lou, B. B. Huang and M. H. Whangbo, *Journal of Physical Chemistry C*, 2014, **118**, 12133-12140.

27. L. Han, P. Wang, C. Z. Zhu, Y. M. Zhai and S. J. Dong, *Nanoscale*, 2011, **3**, 2931-2935.

28. H. Xu, H. M. Li, J. X. Xia, S. Yin, Z. J. Luo, L. Liu and L. Xu, *Acs Applied Materials & Interfaces*, 2011, **3**, 22-29.

29. Y. Y. Li and Y. Ding, *Journal of Physical Chemistry C*, 2010, **114**, 3175-3179.

30. L. Ge, C. C. Han, J. Liu and Y. F. Li, *Applied Catalysis a-General*, 2011, **409**, 215-222.

31. T. Hua and F. Wai Yip, *Chemical Physics Letters*, 2005, **406**, 289-293.

32. S. Glaus and G. Calzaferri, *Photochemical & Photobiological Sciences*, 2003, **2**, 398-401.

33. J. Tejeda, N. J. Shevchik, W. Braun, A. Goldmann and M. Cardona, *Physical Review B (Solid State)*, 1975, **12**, 1557-1566.

34. C. C. Han, L. Ge, C. F. Chen, Y. J. Li, Z. Zhao, X. L. Xiao, Z. L. Li and J. L. Zhang, *Journal of Materials Chemistry A*, 2014, **2**, 12594-12600.

35. M. S. Zhu, P. L. Chen, W. H. Ma, B. Lei and M. H. Liu, *Acs Applied Materials & Interfaces*, 2012, **4**, 6386-6392.

36. L. Xinhui, H. Jinlin, L. Jiajia, H. Yong, S. Yong, Y. Haijian, T. Guoxiu and Q. Haisheng, *Materials Letters*, 2013, **91**, 129-132.

37. J. Cao, B. D. Luo, H. L. Lin, B. Y. Xu and S. F. Chen, *Journal of Hazardous Materials*, 2012, **217**, 107-115.

38. D. Lihong, T. Shanshan, Z. Junyi, Z. Peiying, Z. Lifan and T. Fengwei, *Materials Letters*, 2013, **91**, 245-248.

Synthesis of biocompatible silver-filling organic compounds nanoparticles via bio-reduction using an extract from cherry leaves.

Abstract

Abstract

Multi-functional silver nanoparticles are in significant demand in both fundamental and practical studies thanks to their distinctive physicochemical properties. Silver nanoparticles can be synthesised by physical, chemical and biological methods, but biological syntheses are environmentally friendly, and furthermore there is no need for high pressure, high temperature and toxic chemicals. Silver nanoparticles covered with organic compounds are synthesised by mixing a leaf extract from Yoshino cherry with aqueous solution of silver nitrate. The particles show their high mono-dispersibility in water and biocompatibility thanks to the compounds covering the silver nanoparticles, and high surface enhanced Raman scattering activity owing to the core silver nanoparticles. The antibacterial activity of the particles is also investigated using *Escherichia coli* and *Bacillus subtilis*.
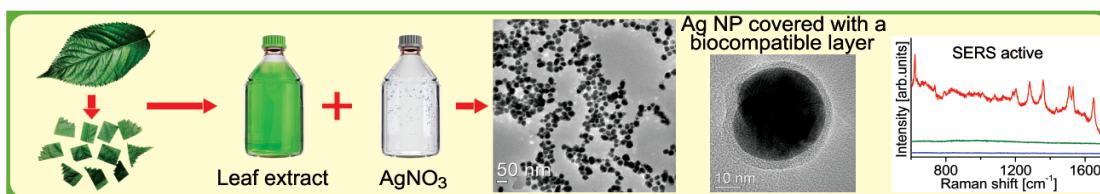
Introduction

2.1 Introduction

Prunus yedoensis belongs to Rosaceae family and is commonly called Yoshino cherry (Sakura). It is a deciduous flowering cherry plant, which is widely cultivated in various countries[1][2]. It occurs as natural hybrid flowering cherry plant in Japan and is widely cultivated in other temperate countries. It is a hybrid cherry probably between *Prunus speciosa* as father plant and *Prunus pendula f. ascendens* as mother[3]. A variety of *Prunus* species have been extensively studied since they possess admirable medicinal properties. Traditional medicine such as 'Yaeng-Pi' and 'Hua-Pi', which have been used for the treatment of cough, urticaria, pruritus, dermatitis, asthma, and measles [4][5], are in fact produced from *Prunus yedoensis*. The antioxidant and antiviral activities and the antihyperglycemic effect have also been intensively examined [6][7]. The tree bark as a Japanese folk medicine is used for detoxification and in additional used as a cough medicine, as an expectorant, to ease swelling, and to apply sores. Cherry bark extracts has been used to produce a commercial product called Brocin, which is being used to treatment coughs and mucus. Flavonoid glycosides present in the extracts are believed to be the probable reason for its medicinal functions. It was reported that *P. yedoensis* contains a large amount of different types of flavonoids [8] and the structures of the flavonoids contained in mature leaves of *P. yedoensis* were identified as 5,4′-dihydroxy-7-methoxyisoflavone 4′-O-glucoside (prunetrin), 5,7,3′,4′-tetrahydroxyflavonol 3-O-glucoside (isoquercitrin), catechin, epicatechin, cyanidin 3-O-monoglucoside (chrysanthemin), and procyanidin. [9][10]. Based on the admirable properties like presence of valuable flavonoid glycosides in the plant and its various extracts, considering their outstanding properties; e.g., anticancer, antihyperglycemic [7] antioxidant [11] anti-inflammatory [12] [13] vasorelaxant [14] and antifungal precursory [15] effects and activities, in the present study the leaf extract of this medicinal plant species was used to exploit its properties in the synthesis of Ag NPs (silver nanoparticles) and later as synthesised particles used in various applications.

Highlights:

- A green reliable method where no toxic chemicals, high temperature or pressure or any sophisticated conditions was utilized during the synthesis.
- The temperature variations during the reaction had an absolute influence on the synthesis of nanoparticles in order to maintain their size and shape.
- Re-nucleation and agglomeration of nanoparticles was prevented up to certain limit by following the new protocol.
- Definite organic compounds capping layer was formed around the particles, which was the prime reason for biocompatibility.
- Stability of particles in aqueous solution for several weeks.
- High SERS performance.
- Antibacterial efficacy is quite considerable that even at low concentrations as-synthesized particles exhibited delay in growth of bacteria.

Experimental methods

2.2 Methodology – 1

The fresh plant leaves of *Prunus yedoensis* were collected from the Kawagoe Campus, Toyo University, Japan, and washed with millipore water to remove surface filth. The leaves were cut into small pieces; approximately 1.0 x 1.0 cm. 10g of the leaf pieces were boiled in 100ml deionized water for 15 min and filtration of the mixture was carried out by using filter paper (Whatman Cat No 1002-185) to obtain fresh aqueous leaf extract. The leaf extract was refrigerated at $4\,^{\circ}C$ for future use. 20 ml of the aqueous leaf extract was mixed with 60 ml of 1mM aqueous solution of $AgNO_3$ (Sigma-Aldrich, Japan) under continuous stirring at $37\,^{\circ}C$ for 60 min. This mixture centrifuged at 15000 rpm for 30 min to obtain the Ag NPs. Thus obtained pellet was purified after dispersing it in millipore water, followed by centrifugation at 15000 rpm for 30 min.

Results and Discussion

The plasmon resonance peak recorded by using UV-Vis-NIR spectroscopy was the primary confirmation of the synthesised nanoparticles. The leaf components are responsible for the reduction of the $AgNO_3$ to synthesize Ag NPs. A typical observation and study was done using Transmission Electron Microscope analysis, in order to understand the nucleation and growth of the synthesised particles when different parameters were changed in the synthetic protocol. **Figure 1** shows the transmission electron micrograph, it is noticed that the particles were aggregated moreover small particles were formed, revealing that the nucleation and growth of the crystal is not constant. In order to over come this issue certain experiments were performed to determine the factors affecting the synthesis mechanism. Here with, a conclusion step was followed to determine the crystal growth based on alteration in temperature and achieved a considerable results.
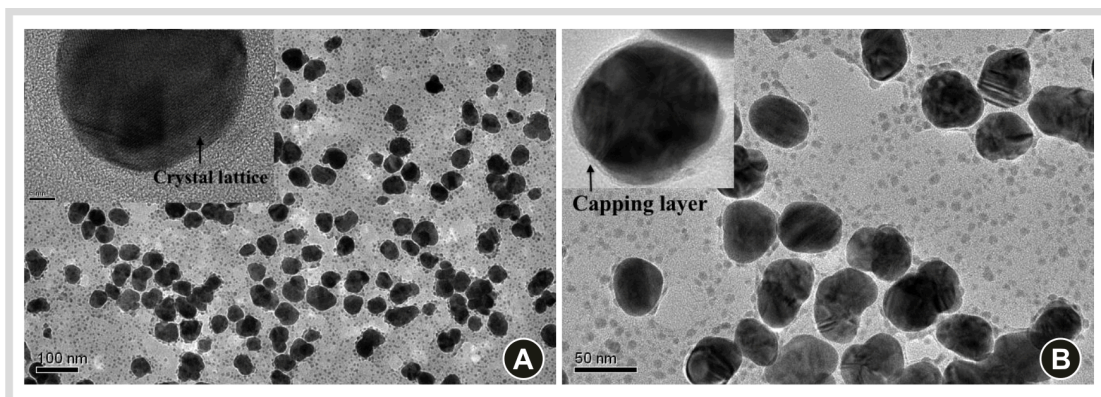
Figure 1 (a) Wide view of nanoparticles and small particles of different sizes were also present, inset – crystal lattice fringes (b) Nanoparticles covered with a capping layer, inset- capping layer around the particle.

2.3 Methodology – 2

Fresh plant leaves of *Prunus yedoensis* were collected from the Kawagoe Campus, Toyo University, Japan, and washed with millipore water to remove surface filth. The leaves were cut into squares of approximately 1.0 × 1.0 cm. 10 g of the leaf pieces were boiled in 100 ml millipore water for 15 min and filtration of the mixture was carried out using filter paper (Whatman Cat No 1002-185) to obtain a fresh aqueous leaf extract. The leaf extract was refrigerated at 4 °C. 20 ml of the aqueous leaf extract was mixed with 60 ml of 1 mM aqueous solution of $AgNO_3$ (Sigma-Aldrich) rigorously at 4 °C. The mixture (pH 5.8) was transferred to conical flask which was at 37° C in water bath and the temperature raise was observed from 4 °C to 30 °C within 5 min, and from 30 °C to 37 °C at a rate of 273.25K min^{-1} for 55 min under continuous stirring. This mixture was centrifuged at 15000 rpm for 30 min and finally a pellet was obtained. The pellet was purified after dispersing it in millipore water, followed by centrifugation at 15000 rpm for 30 min. Thus obtained nanoparticles were well characterized and further analysed for their biocompatibility, surface enhanced Raman scattering (SERS), and anti-bacterial efficacy.

Characterisation

2.4 Characterization of Ag NPs

The optical properties of the as-synthesized NPs were characterized by an ultraviolet-visible (UV-Vis) spectrophotometer (DU 730, Beckman Coulter) in the range from 200 to 1000 nm at a resolution of 1 nm. The morphology and structures of the Ag NPs were studied using a transmission electron microscope (TEM) (JEM2200FS, JEOL) at an acceleration voltage of 200 kV. Particles' samples for TEM observation were prepared drying a droplet of a particles' suspension on a carbon coated copper grid (Cu 200 mesh, JEOL) at room temperature. The crystal nature of the particles was determined by an X-ray diffractometer (XRD) (Smart Lab, Rigaku), using a Cu Kα X-ray with a wavelength of 0.154 nm, a voltage of 45 kV and a current of 200 mA, and employing the grazing-incidence X-ray diffraction procedure with scanning 2θ from 30° to 90° at 6.05 degrees per min at an incident angle of 0.01 degree. The zeta potential of the Ag NPs dispersed in millipore water were measured (pH 6) using a particle analyser (Zeta Nanosizer, Nano ZS, Malvern). The elemental composition of the particles was analysed by energy dispersive X-ray spectroscopy (EDS) (JEM2200FS, JEOL) at an accelerating voltage of 200 kV. The chemical functional groups of the organic compounds capping the particles were analysed by Fourier transform infrared spectroscopy (FT-IR) (Nicolet iS50, Thermo Fischer Scientific), scanning the samples from 400 to 4000 cm^{-1} at a resolution of 4 cm^{-1}. The particles were dried in vacuum and samples for FT-IR measurement were prepared by the KBr pellet method [16]. The elemental and chemical bonding states of the particles were studied by XPS (Axis-HIs, Kratos analytical). Argon ion etching of the samples was performed for 90 s at 1.33×10^{-5} Pa. Pre and post-etching measurement of the particles was recorded at 3.99×10^{-7} Pa to analyse the composition of the core particles and capping compounds around the particles.

Results
and
Discussion

2.5 Results and Discussion

UV- Vis - NIR spectroscopy

Silver nanoparticles were successfully synthesised by mixing a leaf extract from *Prunus yedoensis* with an aqueous solution of 1 mM $AgNO_3$. The colour of the solution changed from pale green to brown (**Figure 2 (a)**), which is an indication of the occurrence of the reduction reaction, noting that the brown colour is induced by the surface plasmon resonance (SPR) of Ag NPs [17]. The time variation of the absorption spectrum of the solution during the synthetic procedure is shown in **Figure 2 (b)**.
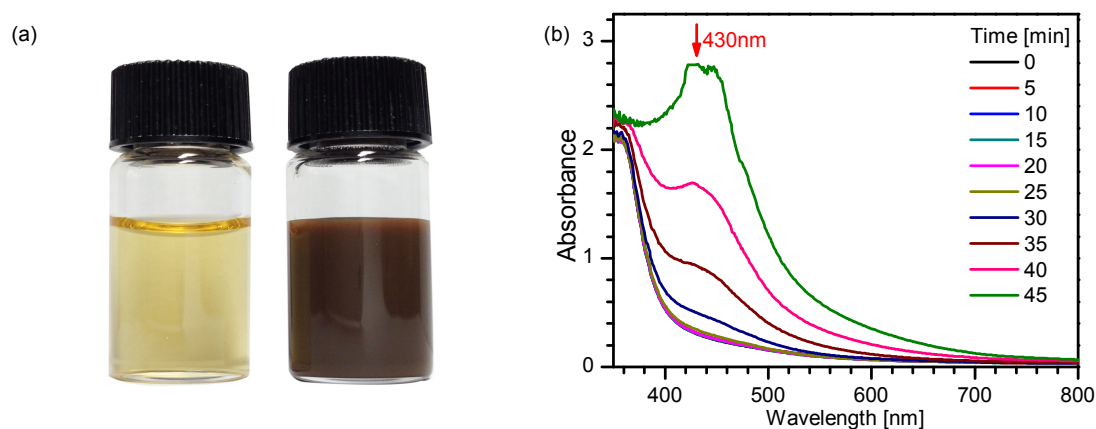
Figure 1. Photograph of aqueous solution of a leaf extract and purified nanoparticles and the time variation of the absorption spectrum of the aqueous solution during the synthetic process of nanoparticles. A leaf extract from *P. yedoensis* was mixed with aqueous solution of silver nitrate at time 0. (a) Photograph of aqueous solution of a leaf extract (left) and purified nanoparticles (right). The colour changed from pale green at time 0 to brown 60 min after mixing. (b) Time variation of the absorption spectrum of the aqueous solution. The intensity of the peak in the absorption spectrum at around 430 nm gradually increased. Note that the peak intensity of the spectrum reached the unmeasurable range of the UV-Vis-NIR spectrophotometer 45 min after mixing.

It is supposed that Ag NPs were gradually synthesised judging by the increase in the intensity of the SPR peak at around 430 nm [18] (**Figure 3**). In other words, the leaf extract from *Prunus yedoensis* acted as a reducing agent of $AgNO_3$.
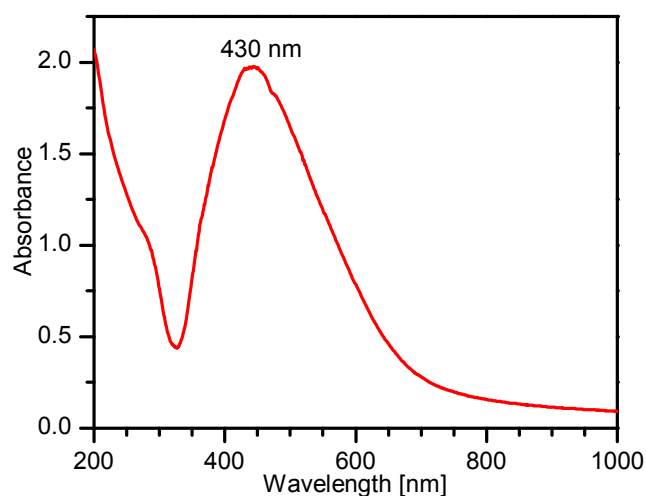
Figure 3 Absorption spectrum of purified Ag NPs dispersed in millipore water.

Transmission electron microscopy and scanning electron microscopy

TEM images of as-synthesized particles are shown in **Figure 4**. Each particle was covered with a layer of some material, the component of which will be characterised later. The core particles were not perfectly spherical, but crystallised (**Figure 4(c), 2(d)**). According to the TEM image (**Figure 4(c)**), the selected area electron diffraction image (**Figure 4(d)**), The diameter of a core silver particle, which was measured from TEM images targeting at least 100 particles, was 26.3 ± 6.4 nm (see **Figure 5** for the distribution of the diameter of the core particles), whereas the thickness of the layer covering the particles was 2.6 ± 0.5 nm (see **Figure 6** for the distribution of the thickness of the layers). Note that particles of the order of several nanometers were also observed. In the **Figure 7** scanning electron microscope image shows the as-synthesised particles were covered with a layer of material.
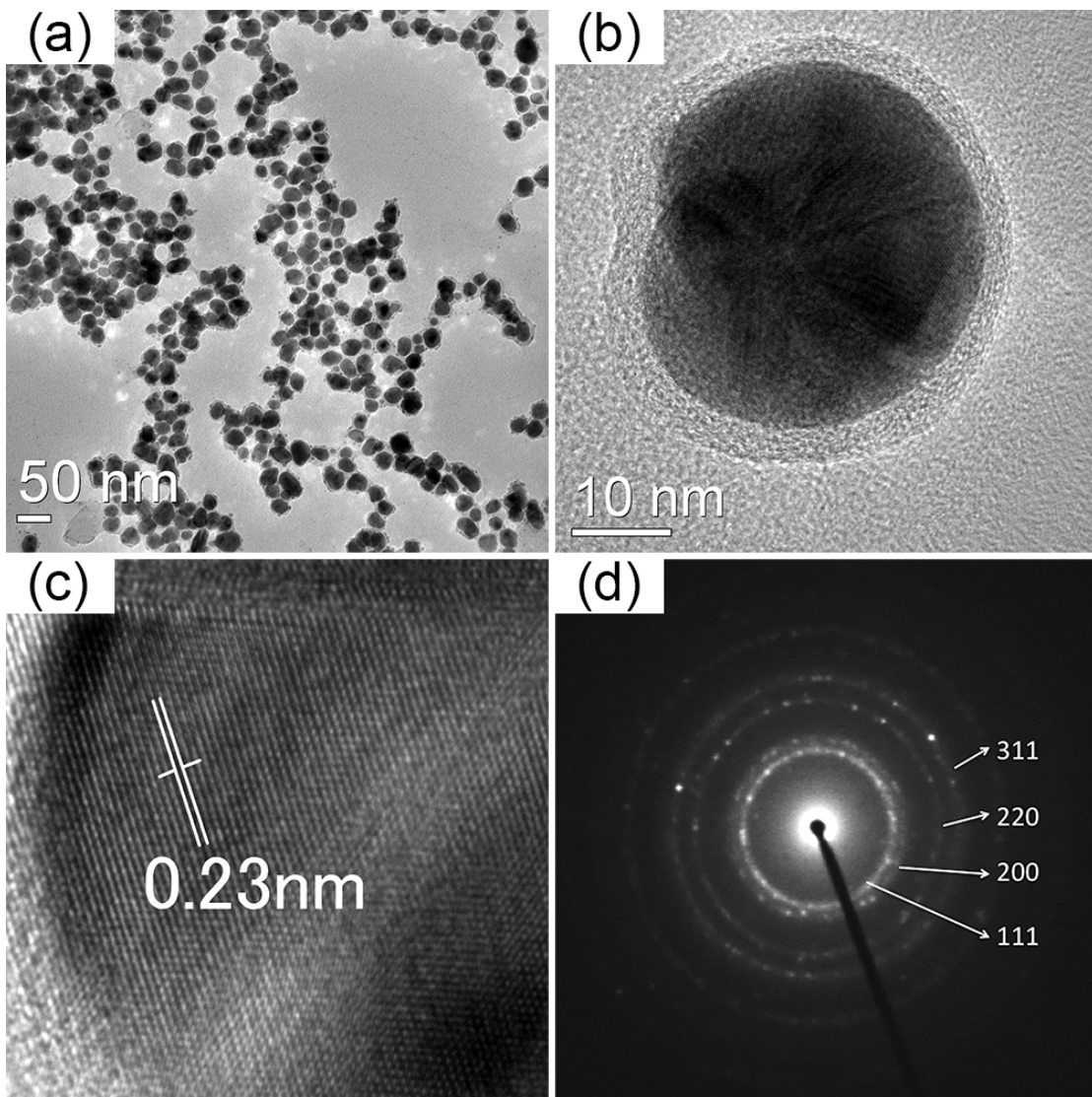
Figure 4 TEM and SAED images of nanoparticles. (a) Wide view of nanoparticles. The diameter of each particle is quite uniform. (b) Magnified image of a nanoparticle. A core particle is covered with a layer of some materials. (c) Lattice fringes. The gap between two neighbouring fringes is 0.23 nm, which coincides with that of silver. (d) SAED image. The indices indicate that the core particle is composed of silver.
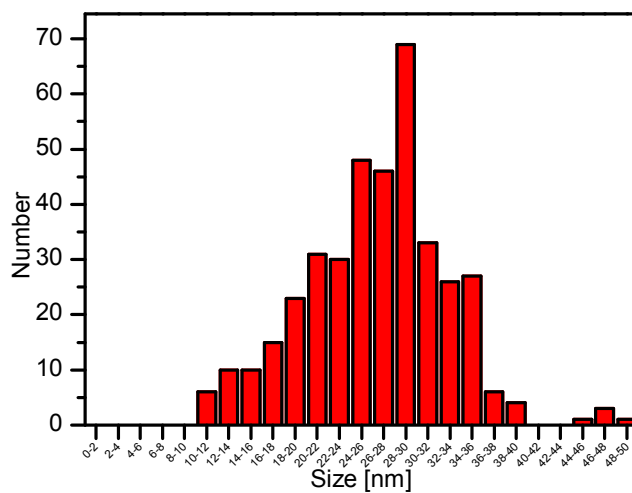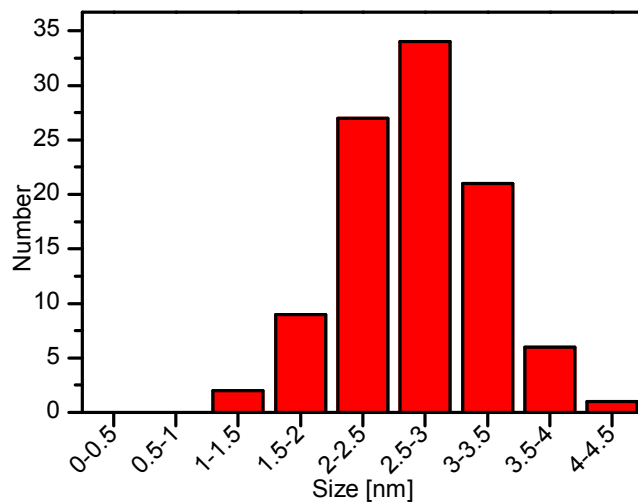
Figure 5 Distribution of the diameter of the core Ag NPs.

Figure 6 Distribution of the thickness of capping layers

SU8000 5.0kV x60.0k SE(U)   500nm
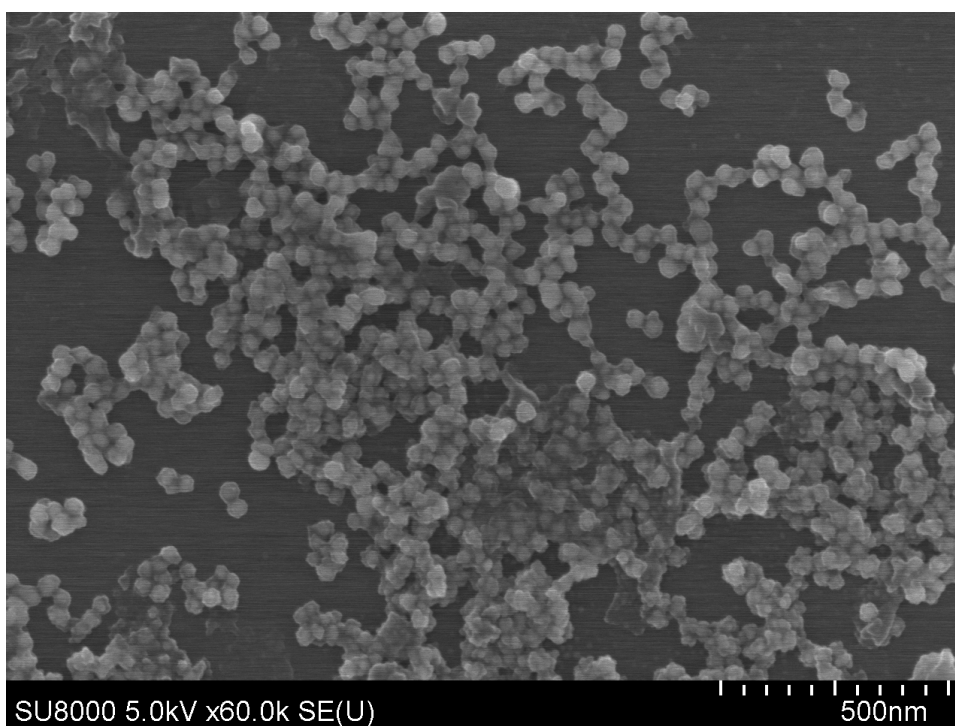
Figure 7 Wide view of Ag NPs covered with a capping layer

X-ray diffraction

The crystalline structure of the core particles was face-centered cubic (FCC), noting that the X-ray diffractogram was in good agreement with the standard data of the Joint Committee on Powder Diffraction Standards (JC-PDF) file 4-783 [19]. It showed well-defined 2θ peaks at 38.14°, 44.48°, 64.42° and 77.64°, which, respectively, correspond to (111), (200), (220), and (311) reflections (see **Figure 8**). This data determine the crystal geometry of the core Ag NPs to be face-centred cubic. The metallic nature of the Ag NPs confirmed by the XRD profile coincides with the previous study [20]. According to the Debye-Scherrer equation [21] the mean size of a crystal domain was calculated to be 10.3 nm based on the full width at the half maximum (FWHM) of the (111) Bragg's reflection.
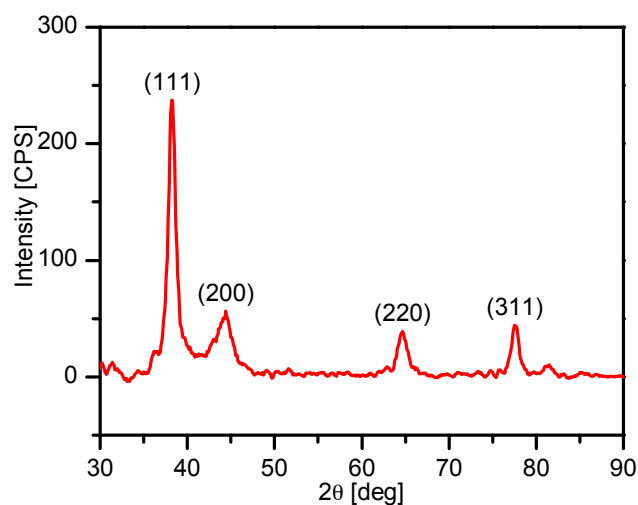
Figure 8 X-ray diffractogram of as-synthesised nanoparticles.

Zeta potential

The Ag NPs were stably dispersed in water without any serious coagulation, judging by the visual observation of the solution (see **Figure 2**). In general, when the absolute value of the zeta potential of particles is lower than 20 mV, the particles tend to be unstable in the solution and the precipitation of particles occurs [22], whereas the particles are stably dispersed when the absolute value of the zeta potential is higher than 20 mV [23]. In the present case, The zeta potentials of the particles in millipore water measured immediately and 4 weeks after purification were, respectively, - 32.0 ± 6.3 and - 35.4 ± 7.0 mV and as a result, the Ag NPs were stably dispersed in millipore water (see **Figure 9**) [24].
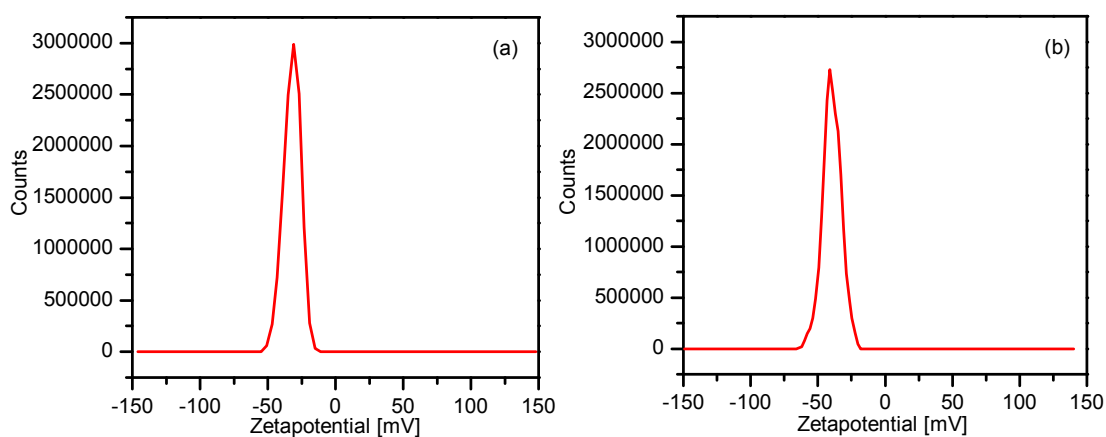
Figure 9 Distributions of the zeta potentials of particles in millipore water measured (a) immediate after purification of Ag NPs and (b) 4 weeks after purification.

Energy dispersive X-ray spectroscopy

The EDS spectrum showed a strong signal of Ag La at 3.0 keV, which confirms that the inner particles are composed of silver (**Figure 10**). The Carbon signal was detected from the organic layer capping around the particles and the grid, the Copper signal was detected from the grid.
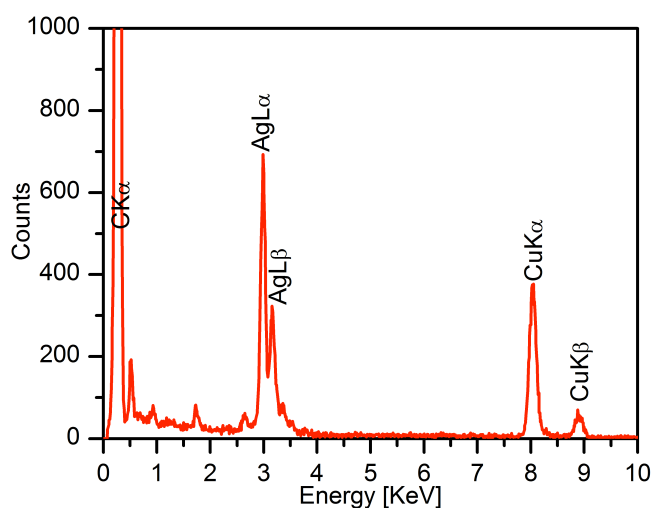

Figure 10 Elemental analysis of nanoparticles by EDS.

Fourier transform infrared spectroscopy

According to the FT-IR spectrum shown in **Figure 11**, the functional groups on the capping layers were very similar to those of the leaf extract. The peaks at around 3400 cm^{-1} (corresponding to O–H), 1600 cm^{-1} (C=O, C=C) and 1000 cm^{-1} (C–O) are in accordance with those of some flavonoids such as cathechin, epicathechin, isoquercitrin and cyanidin compounds [25-28] and therefore it is supposed that the capping layers were composed of flavonoids.
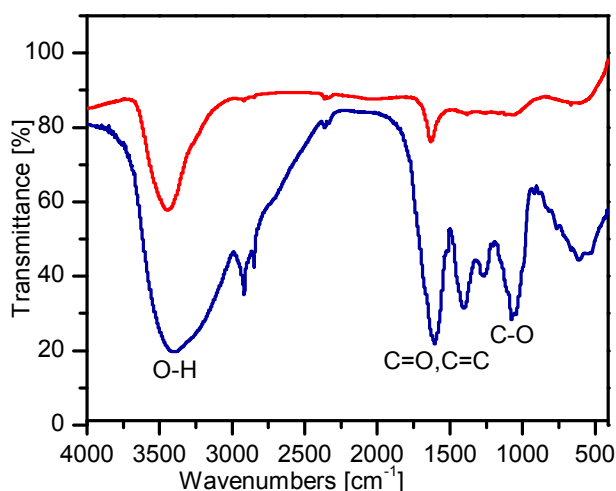

Figure 11 FT-IR spectra of as-synthesised particles (represented in red) and the leaf extract (in blue). The peaks at around 3400, 1600 and 1000 cm^{-1}, respectively, correspond to (O–H), (C=O, C=C) and (C–O).

X-ray photoelectron spectroscopy

The XPS analysis depicts the elementary composition of the particles and the atomic percentage of carbon and silver were determined. According to the pre-etching and post-etching XPS data; that is, the intensities of the peaks of Ag3p, Ag3d, O1s and C1s (**Figure 12 (a)**), the present particles are composed of Ag NPs conjugated with some materials containing carbon.

According to the Gaussian-Lorentzian curve fitting, in **Figure 12 (c)** the pre-etching peaks of C1s correspond to a binding energy of 284.9 eV. It is therefore supposed that alkyl carbon (C-C) or hydro carbon (C-H) were detected on the surface of the compounds capping the Ag NPs. The pre-etching and post-etching XPS data were analysed to define the chemical nature of pristine Ag NPs. **Figure 12 (b)** shows peaks of Ag3d core levels and the details are

summarised in **Table 1** [29]. The peaks of $Ag3d_{5/2}$ and $Ag3d_{3/2}$ were fitted with Gaussian-Lorentzian curves. The pre-etching data indicate the existence of Ag-O/Ag-C, whereas the post-etching data metallic Ag, noting that the binding energies of the pre-etching data shifted towards higher ones after etching, which confirms the conversion of Ag-O/Ag-C into metallic Ag [30]. The FWHM values of the pre-etching data (broad peak) were lower than those of the post-etching data (narrow peak), which confirms the switching of Ag-O/Ag-C species to Ag-metal [31]. The atomic percentages of silver and carbon were summarised in **Figure 13**.

	Ag 3d $_{5/2}$ B.E - FWHM	**Ag3d $_{3/2}$** B.E - FWHM
Pre-etching	367.80 - 0.98	373.90 - 0.95
Post-etching	367.98 - 0.74	373.99 - 0.76

Table 1 Pre-etching and post-etching data of Ag3d $_{5/2}$ and Ag3d $_{3/2}$, representing the peak position of the binding energies (B.E.), and the full width at the half maximum (FWHM).
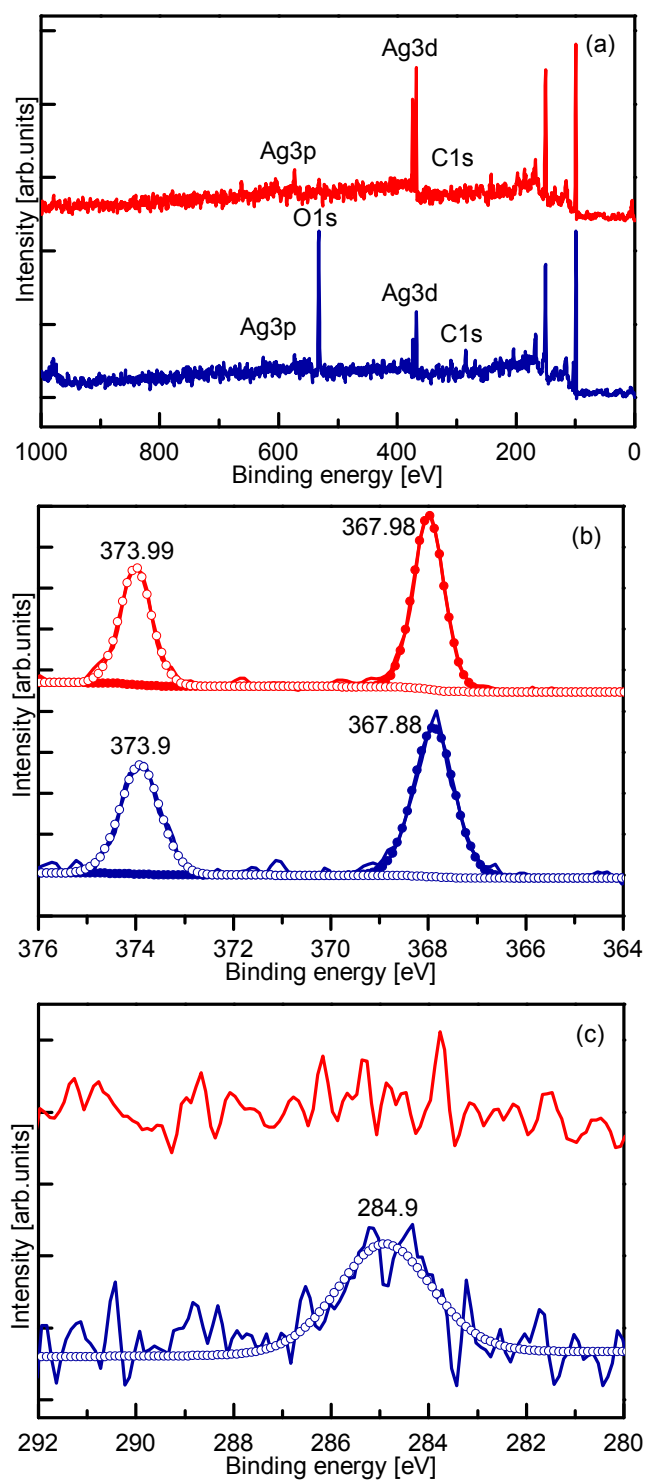
Figure 12 XPS spectra of as-synthesised particles measured under pre-etching (represented in blue) and post-etching (red) conditions. (a) Overall spectra; (b) Ag3d; (c) C1s.
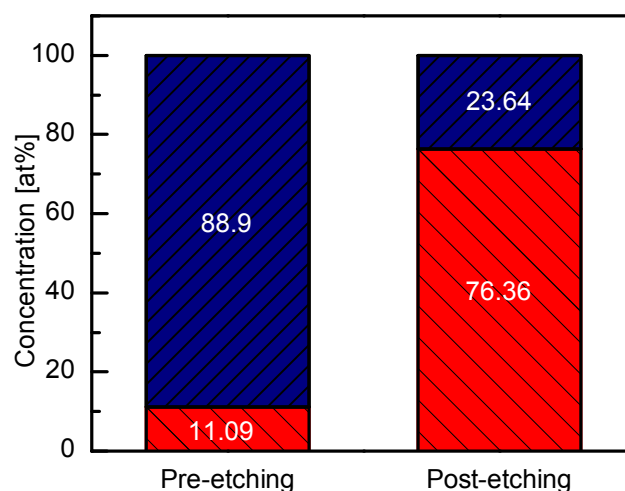
Figure 13 Atomic percentages of silver and carbon composing nanoparticles. Elemental analyses were carried out by XPS before and after etching of the nanoparticles. The red bars represent silver, whereas the blue ones carbon.

Biocompatibility investigation by an Alamar blue assay, cell staining and hemolysis study

A test cell line; L929, was cultured in a 25 cm^3 flask, which contained Dulbecco's modified eagle media (DMEM) (Gibco, Life Technologies) supplemented with 10% foetal bovine serum and 1% penicillin-streptomycin. The cells were seeded in 96-well plates with DMEM at a cell number density of 3×10^3 and 5×10^3 cells per well (CPW) and incubated for 48 and 24 h, respectively. Then, the media were removed and replaced by fresh ones and the cells of 3×10^3 and 5×10^3 CPW were incubated in the presence of a different concentration of particles; 0, 10, 20, 40, 80 and 100 µg mL^{-1}, and a different concentration of the aqueous solution of the leaf extract; 0, 10, 20, 40, 80 and 100 µL mL^{-1} for 48 and 24 h, followed by treatment with an Alamar blue reagent for 3 h. The incubation was performed in an atmosphere of 5% CO$_2$ at 37 °C. The fluorescence intensity of the solution was then measured using a multi detection micro plate reader (Powerscan HT, Dainippon Sumitomo pharma Co., Ltd, Japan) with an excitation wavelength of 530 nm and emission wavelength of 590 nm. The cells in the media in the absence of particles acted as the positive control. The metabolic activity and proliferation of cell line L929 in the presence of Ag NPs were analysed and **Figure 14 (a)** shows the cell

viability in the presence of the Ag NPs. Even in the case of high concentrations of Ag NPs used in the assay; i.e., 80 and 100 µg ml^{-1}, the cell viability was still high, whereas in the case of the other lower concentrations of Ag NPs, the particles' cytotoxicity was very low. Note that the leaf extract also showed its high biocompatibility (**Figure 14 (b)**). The present result is in good agreement with the one previously reported by Moulton et al [32], where the biocompatibility of of green synthesized Ag NPs was investigated using HaCaT cells. There have been several reports showing evidence of a high biocompatibility of surface modified or capped Ag NPs [33-35], whereas on the contrary, naked Ag NPs exhibited cytotoxicity and genotoxicity [36-38].
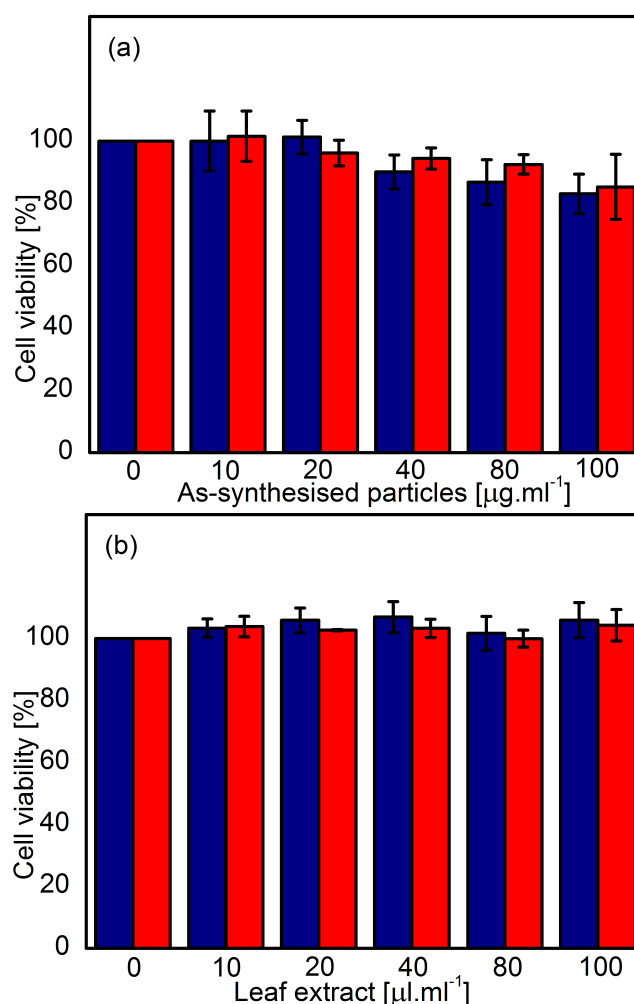

Figure 14 Viability of cell line L929 estimated by an Alamar blue assay. (a) Viability of cells cultivated in the presence of Ag NPs. (b) Viability of cells cultivated in the presence of the leaf extract. The blue bars represent the cell viability assessed using 5000 cells per well incubated for 24h, whereas the red ones the cell viability estimated using 3000 cells per well incubated for 48 h.

In addition to the Alamar blue assay, the cell viability of cell line L929 in the presence of a different concentration of Ag NPs was investigated using a fluorescent stain; It was also performed using calcein-AM (Dojindo Molecular Technologies Inc.) and propidium iodide (Dojindo Molecular Technologies Inc.) to determine the cell viability which induce green and red fluorescence, respectively, for alive and dead cells [39]. Initially, cells of 5×10^3 CPW were seeded in a 96-well plate with DMEM and incubated for 24 h in an atmosphere of 5% CO_2 at 37 °C. Then, the media were removed and replaced by fresh ones and the cells of 5×10^3 CPW were incubated with a different concentration of particles; 0, 10, 20, 40, 80 and 100 µg mL^{-1}, and a different concentration of the aqueous solution of the leaf extract; 0, 10, 20, 40, 80 and 100 µL mL^{-1}, for 24 h. 100 µL of calcein AM (2 µmol) / propidium iodide stain (4 µmol) was introduced into each well and the cells were incubated for 15 min. Fluorescence images were captured using a confocal laser scanning microscope (A1si+, Nikon Corp.) with an excitation wavelength of 488 and 561 nm. The confocal fluorescence images shown in **Figure 15** indicates that the present Ag NPs did not promote any adverse effect on the proliferation of the test cell line and leaf extract also did not promote any adverse effect (**Figure 16**).
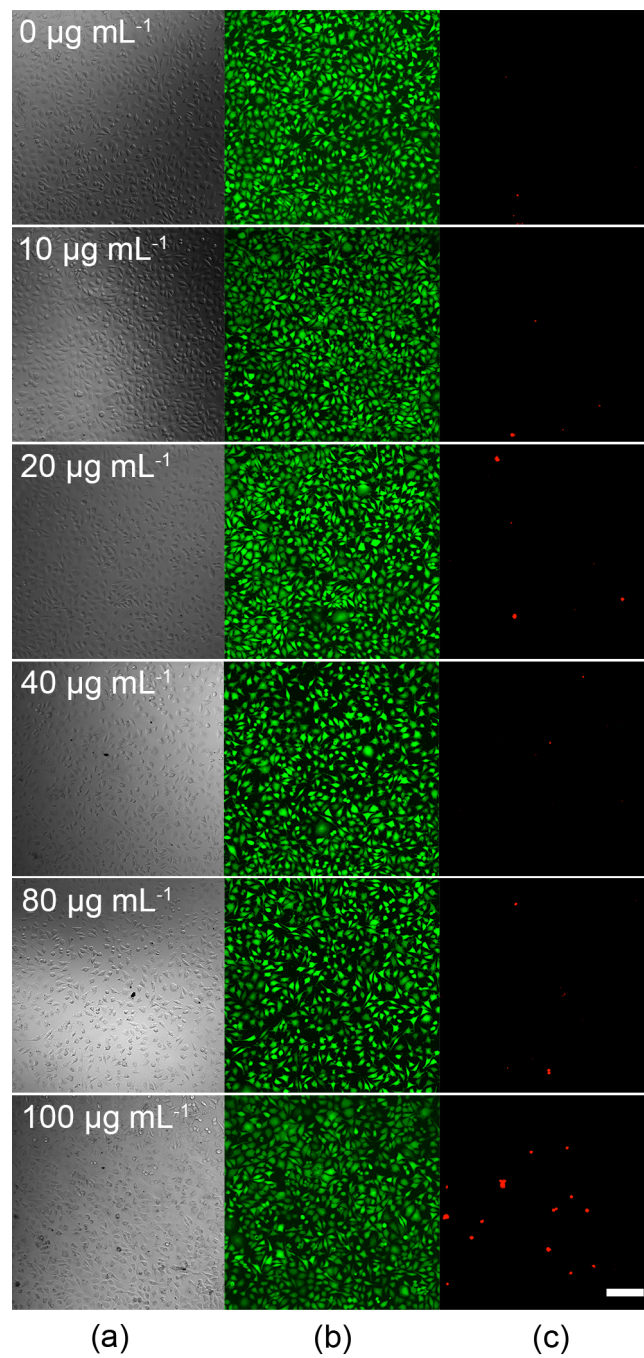
Figure 15 Confocal fluorescence images of cell line L929 in the presence of Ag NPs. (a) Bright field images. (b) Alive cells (green). (c) Dead cells (red). The scale bar represents 200 μm.
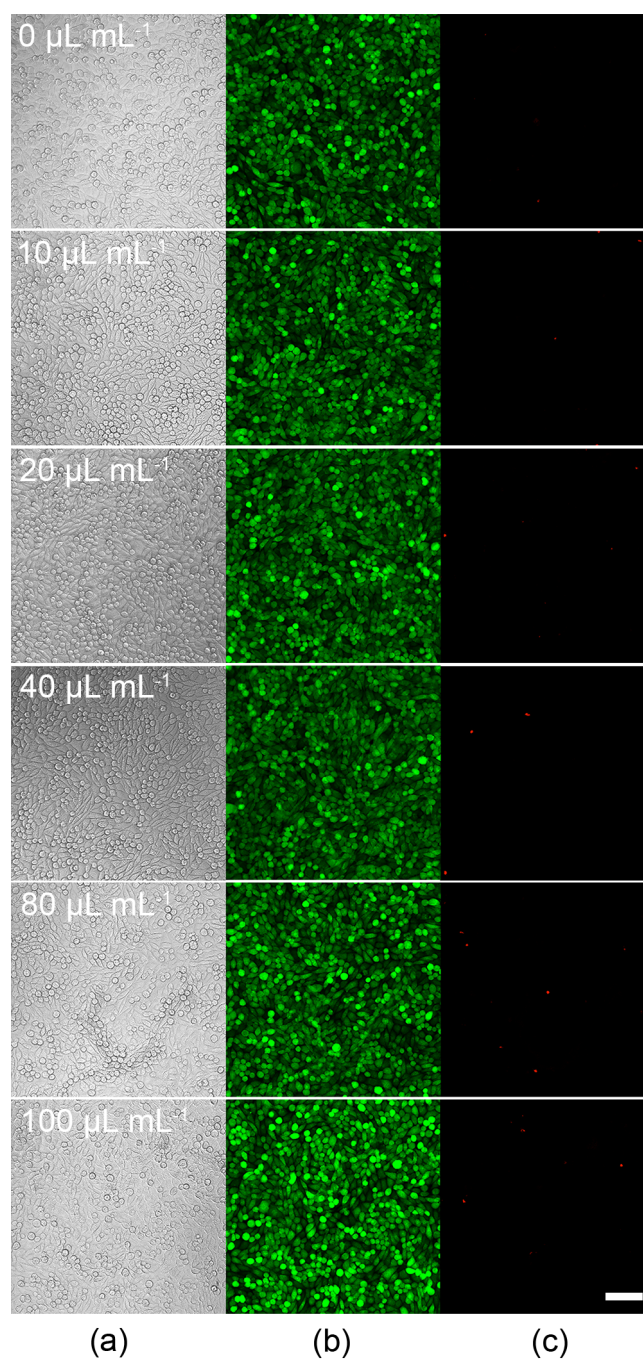
Figure 16 Confocal fluorescence images of cell line L929 in the presence of the leaf extract without any particles. (a) Bright field images. (b) Alive cells (green). (c) Dead cells (red). The scale bar represents 200 µm.

Hemocompatibility of the Ag NPs was also examined using sheep's and rabbits' RBCs for further confirmation of biocompatibility of the Ag NPs and the study was carried out as follows [40]. RBCs were separated from fresh sheep's and rabbit's blood (1 mL) (Nippon Bio-Supp. Centre) and phosphate buffered saline

(PBS) (10 mL) was added to the RBCs, then followed by centrifugation twice at 1500 rpm for 5 min. The RBCs were suspended in PBS (10 mL). The RBCs' suspension (900 µL) was added to the particles/PBS solution (100 µL), the concentration of the particles of which was set at 10, 20, 40, 80 or 100 µg mL^{-1}, and the RBCs' suspension was also added to the leaf extract/PBS solution (100 µL) of 10, 20, 40, 80 or 100 µL mL^{-1}. The solution was introduced into 2 mL centrifuge tubes and incubated under a gentle rotation at 37 ºC for 60 min. The tubes were finally centrifuged at 1500 rpm for 5 min at 20 ºC and the absorption of incident photons of 540 nm wavelength was measured using the UV-Vis-NIR spectrophotometer (DU 730, Beckman coulter). An aqueous solution of RBCs with Triton X-100 (Sigma-Aldrich, Japan) was used as the positive control.

The hemolytic activity of the Ag NPs was determined by the amount of hemoglobin released from the RBCs in the presence of Ag NPs, which is shown in **Figure 17**. Hemolysis of the Ag NPs and leaf extract which was normalised by the positive control [41], was only 10 % even when the concentration of Ag NPs was as high as 100 µg ml^{-1}. We suppose that the hemocompatibility of the Ag NPs was high, thanks to the organic compounds probably flavonoids capping the Ag NPs [42] and therefore we believe that the present Ag NPs can be used for biomedical studies [43].
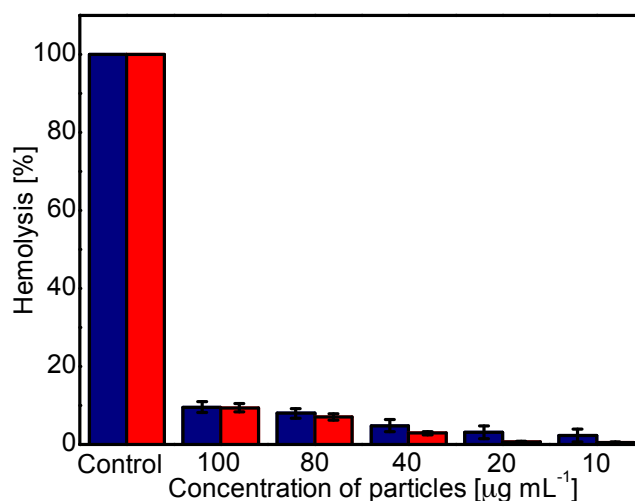

Figure 17 Effect of the concentration of particles on the hemolytic activity. The blue bars represent sheep's RBCs, whereas red ones rabbit's RBCs. RBCs incubated with Triton X-100 acted as the positive control.

Application of Ag NPs in antibacterial activity and SERS assay

Antibacterial assay

To examine the antibacterial activity of the particles, the time variation of the bacterial growth was measured, culturing two bacterial species; *Escherichia coli* at 37 ºC and *Bacillus subtilis* at 30 ºC, in Nutrient broth No.2 (Oxoid) media supplemented with the aqueous solution of particles of 2, 4, 8 or 16 µg mL^{-1}, and with a leaf extract solution of 2, 4, 8 or 16 µL mL^{-1} for 16 h. The optical density (O.D) values at 600 nm were recorded every 30 min using an OD-Monitor (C&T, Taitec Corp.) and the growth curves were obtained.

The time variations of the bacterial growth for up to 4 h 30min are shown in **Figure 18 (a) (b)**. **Figure 19 (a) (b)** shows the time variations of the bacterial growth for 16 h. The growth of both *Bacillus subtilis* (Gram-positive) and *Escherichia coli* (Gram-negative) was reduced in the presence of Ag NPs even when the concentration of the particles was as low as 16 µg ml^{-1}, noting that the antibacterial effect of the leaf extract was not significant (**Figure 19 (c) (d)**). It is therefore supposed that the present Ag NPs possess some antibacterial activity, which corroborates with the study of Liong et al. [44]. Antibacterial activity of the encapsulated silver nanocrystals and their interaction towards both the gram positive and gram negative bacterial cells was previously discussed by Liong et al, which implies to the present report on Ag NPs[44]. I Sondi et al. reported that the bacterial growth was not completely inhibited by Ag NPs in a liquid medium and it was obvious in the present study that the growth rate was delayed as the concentration of the Ag NPs increased [45; 46].
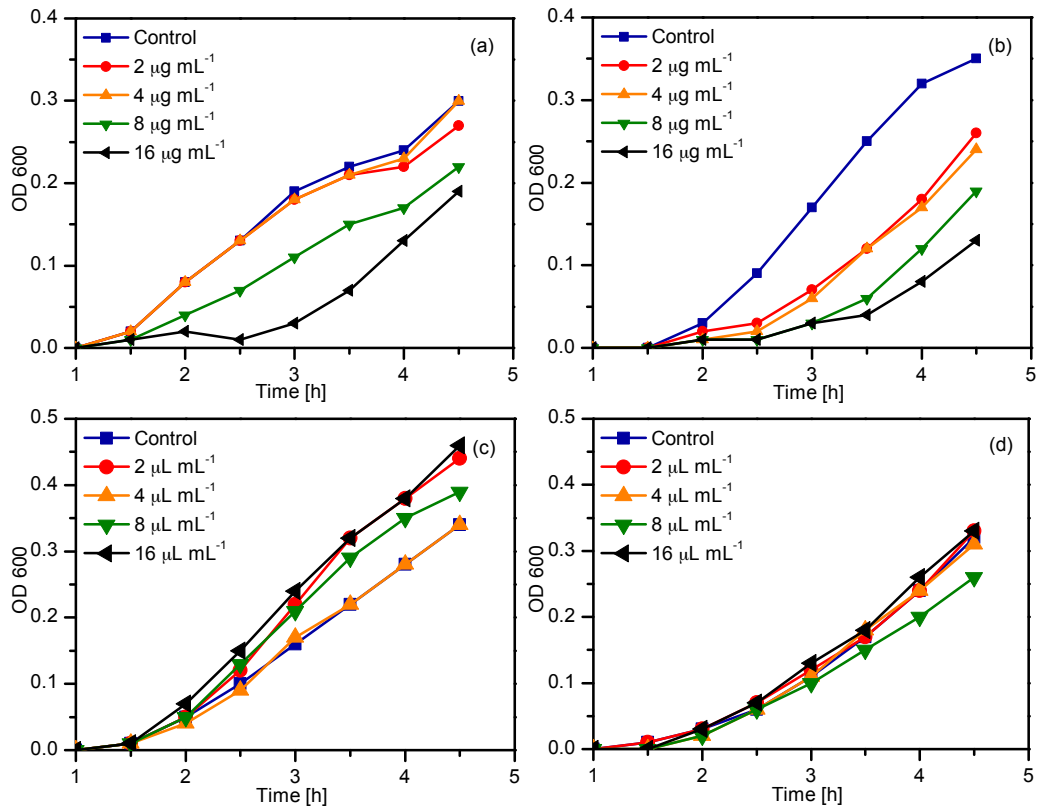
Figure 18 Time variations of the growth of bacteria. (a) Growth of *Escherichia coli* in the presence of Ag NPs. (b) Growth of *Bacillus subtilis* in the presence of Ag NPs. (c) Growth of *Escherichia coli* in the presence of the leaf extract. (d) Growth of *Bacillus subtilis* in the presence of the leaf extract.
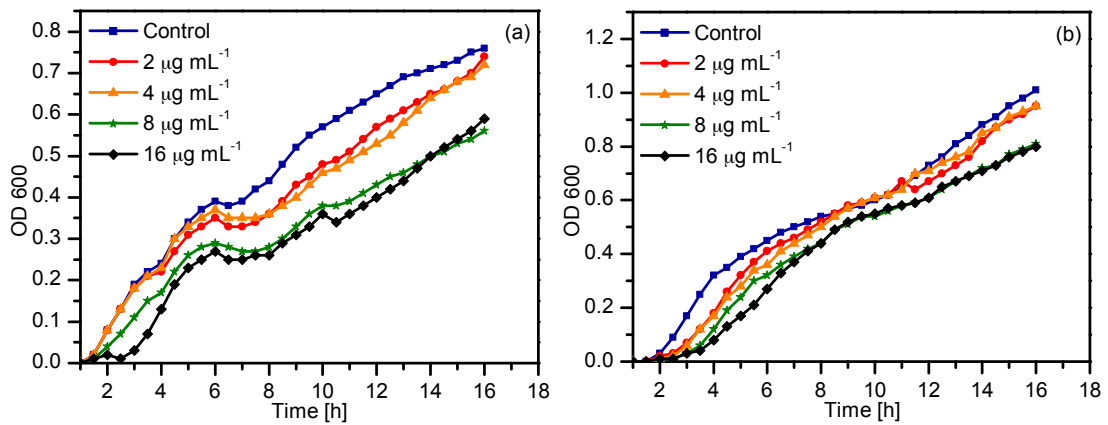

Figure 19 Time variation of the growth of bacteria. (a) *Escherichia coli* (b) *Bacillus subtilis*.

Surface enhanced Raman scattering

The SERS characteristics were investigated using an aqueous solution of rohdamine B. 0.1 mM rohdamine B solution was dropped onto dried Ag NPs and a layer of the leaf extract placed on a glass substrate and Raman spectra were obtained using a micro-Raman spectroscopic system (Lab Ram HR800UV, Horiba Jobin Yvon S.A.S.) with an excitation wavelength of 633 nm. The spot diameter and power of the laser beam were, respectively, 2 μm and 48 μW and the spectra were obtained with a 2-sec integration.

Raman spectra of an aqueous solution of rhodamine B, which was dropped onto Ag NPs placed on a glass substrate, was obtained, the result of which is shown in **Figure 20**. It is clearly shown that Raman signals were greatly enhanced in the presence of Ag NPs and therefore the present particles are highly SERS active, whereas there was no recognizable signals of rhodamine B when it was dropped on the surface of the glass substrate and the leaf extract alone.

Raman shift (cm-1) [47]		
Lit	Ag NPs	Assignment
1648	1648	Aromatic C−C stretching
1529	1530	
1506	1507	
1433	1437	
1356	1358	
1280	1280	C−C bridge band stretching
1201	1201	Aromatic C−H bending
620	622	Aromatic bending

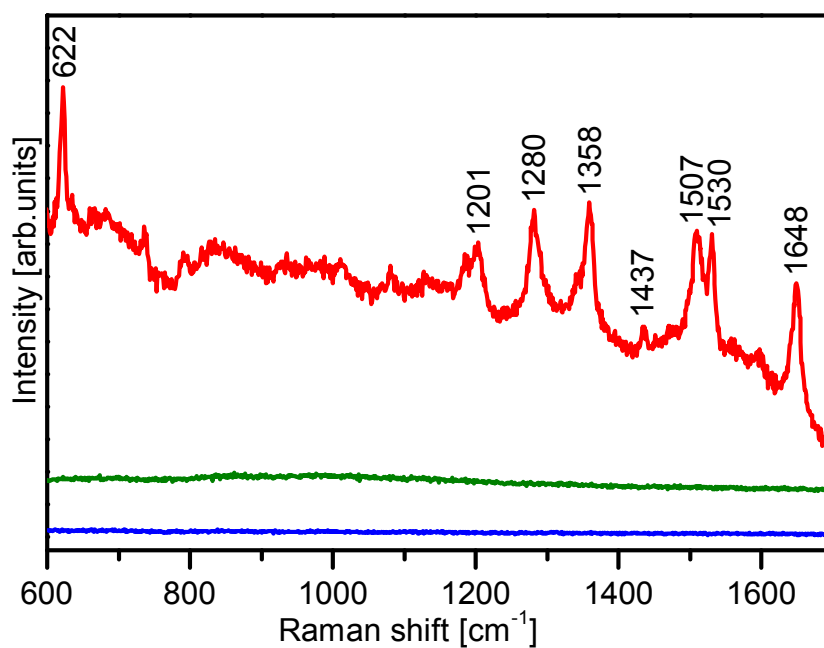**Table 2** Characteristic raman signal peak positions of rhodamine B of

Figure 20 Raman spectra of 0.1 mmol aqueous solution of rhodamine B. The red curve represents a Raman spectrum of the rhodamine B solution dropped on dried Ag NPs, whereas the green and blue curves the spectra of the solution dropped on a dried leaf extract and on the glass substrate. Sharp peaks at 622, 1201, 1280, 1358, 1437, 1507, 1530, and 1648 cm^{-1} are typical ones of rhodamine B.

Conclusion

2.6 Conclusion

Ag NPs were synthesised by mixing a leaf extract from *P. yedoensis* with aqueous solution of $AgNO_3$. The particles showed their high dispersibility in water, biocompatibility, surface enhanced Raman scattering activity and antibacterial activity. We believe that the significant features possessed by the present Ag NPs were derived from the properties of both organic compounds capping the particles and core particles and therefore the Ag NPs may well be actively utilised in the field of biomedicine; e.g., as nano agents for bio-imaging, nano media for photothermal therapy, nano vehicles for drug delivery and detectors of biomolecules and biomaterials. It is also inferred from the previous and present studies that metal-filling organic compounds nanoparticles may commonly be synthesised via bio-reduction using plants' extracts.

References

References

1. H. Innan, R. Terauchi, N. T. Miyashita and K. Tsunewaki, 1995, **70**, 185-196.

2. M. S. Roh, E. J. Cheong, I. Y. Choi and Y. H. Joung, *Scientia Horticulturae*, 2007, **114**, 121-128.

3. S. Ohta, S. Osumi, T. Katsuki, I. Nakamura, T. Yamamoto and Y. I. Sato, *Journal of the Japanese Society for Horticultural Science*, 2006, **75**, 72-78.

4. D. Ahn, *Illustrated Book of Korean Medicinal Herbs*, Seoul: Kyohak publishing, 1998.

5. J. Kim, *Illustrated Natural Drugs Encyclopedia. color edition*, Seoul: Namsandang, 1997.

6. H. S. Yook, K. H. Kim, J. E. Park and H. J. Shin, *American Journal of Chinese Medicine*, 2010, **38**, 937-948.

7. K. Jo, S. E. Lee, S. W. Lee and J. K. Hwang, *Natural Product Research*, 2012, **26**, 1610-1615.

8. R. Hegnauer, *Biochemistry Systematics and Ecology*, 1973, **1**, 191-197.

9. N. Ishikura, *Phytochemistry*, 1972, **11**, 2555-2558.

10. N. Ishikura, Y. Watanabe and S. Teramoto, *The Botanical Magazine, Tokyo*, 1989, **102**, 547-560.

11. HyunAhJung, HaeYoungChung, AeRaKim and JaeSueChoi, *Archives of Pharmacal Research*, 2002, **25**, 865-872.

12. J. Lee, G. Yang, K. Lee, M. H. Lee, J. W. Eom, I. Ham and H. Y. Choi, *Bmc Complementary and Alternative Medicine*, 2013, **13**, 9.

13. Y. Q. Zhang, L. Guan, Z. Y. Zhong, M. Chang, D. K. Zhang, H. Li and W. Lai, *International Journal of Cosmetic Science*, 2014, **36**, 527-530.

14. K. Lee, I. Ham, G. Yang, M. Lee, Y. Bu, H. Kim and H. Y. Choi, *Bmc Complementary and Alternative Medicine*, 2013, **13**, 6.

15. T. Ito and K. Kumazawa, *Bioscience, Biotechnology, and Biochemistry*, 1995, **59**, 1944-1945.

16. N. B. Colthup, L. H. Daly and S. E. Wiberley, *Introduction to Infrared and Raman Spectroscopy*, Academic press, New york-London, 1964.

17.   P. Mulvaney, *Langmuir*, 1996, **12**, 788-800.

18.   R. R. Naik, S. J. Stringer, G. Agarwal, S. E. Jones and M. O. Stone, *Nature Materials*, 2002, **1**, 169-172.

19.   P. Velmurugan, S. M. Lee, M. Iydroose, K. J. Lee and B. T. Oh, *Applied Microbiology and Biotechnology*, 2013, **97**, 361-368.

20.   S. Elzey and V. H. Grassian, *Journal of Nanoparticle Research*, 2010, **12**, 1945-1958.

21.   P. Scherrer, *Bestimmung der Gro¨ße und der inneren Struktur von Kolloidteilchen mittels Ro¨ntgenstrahlen. Nachrichten von der Gesellschaft der Wissenschaften zu Go¨ttingen*, Mathematisch-Physikalische Klasse, 1918.

22.   A. M. El Badawy, T. P. Luxton, R. G. Silva, K. G. Scheckel, M. T. Suidan and T. M. Tolaymat, *Environmental Science & Technology*, 2010, **44**, 1260-1266.

23.   J. Eastoe, in *Micro Emulsions*, ed. T. Cosgrove, 2005, ch. 5, pp. 77-97.

24.   A. K. Suresh, M. J. Doktycz, W. Wang, J. W. Moon, B. H. Gu, H. M. Meyer, D. K. Hensley, D. P. Allison, T. J. Phelps and D. A. Pelletier, *Acta Biomaterialia*, 2011, **7**, 4253-4258.

25.   M. M. Ramos-Tejada, J. D. G. Duran, A. Ontiveros-Ortega, M. Espinosa-Jimenez, R. Perea-Carpio and E. Chibowski, *Colloids and Surfaces B-Biointerfaces*, 2002, **24**, 297-308.

26.   A. M. Mendoza-Wilson and D. Glossman-Mitnik, *Journal of Molecular Structure-Theochem*, 2006, **761**, 97-106.

27.   J. T. Han, M. H. Bang, O. K. Chun, D. O. Kim, C. Y. Lee and N. I. Baek, *Archives of Pharmacal Research*, 2004, **27**, 390-395.

28.   L. K. Singh, T. Karlo and A. Pandey, *Spectrochimica Acta Part a-Molecular and Biomolecular Spectroscopy*, 2014, **118**, 938-943.

29.   C. D.Wagner, W. M. Riggs, L. E. Davis, J. F. Moulder and G. E. Muilenburg, *Handbook of X-ray Photoelectron Spectroscopy*, Perkin-Elmer Corp., Physical Electronics Division: Eden Prairie, Minnesota, 1979.

30. Y. L. Mikhlin, E. A. Vishnyakova, A. S. Romanchenko, S. V. Saikova, M. N. Likhatski, Y. V. Larichev, F. V. Tuzikov, V. I. Zaikovskii and S. M. Zharkov, *Applied Surface Science*, 2014, **297**, 75-83.

31. T. Miyama and Y. Yonezawa, *Journal of Nanoparticle Research*, 2004, **6**, 457-465.

32. M. C. Moulton, L. K. Braydich-Stolle, M. N. Nadagouda, S. Kunzelman, S. M. Hussain and R. S. Varma, *Nanoscale*, 2010, **2**, 763-770.

33. P. K. Prabhakar, S. Raj, P. R. Anuradha, S. N. Sawant and M. Doble, *Colloids and Surfaces B-Biointerfaces*, 2011, **86**, 146-153.

34. E. I. Alarcon, K. Udekwu, M. Skog, N. L. Pacioni, K. G. Stamplecoskie, M. Gonzalez-Bejar, N. Polisetti, A. Wickham, A. Richter-Dahlfors, M. Griffith and J. C. Scaiano, *Biomaterials*, 2012, **33**, 4947-4956.

35. A. Mandal, V. Meda, W. J. Zhang, K. M. Farhan and A. Gnanamani, *Colloids and Surfaces B-Biointerfaces*, 2012, **90**, 191-196.

36. M. Ahamed, M. S. AlSalhi and M. K. J. Siddiqui, *Clinica Chimica Acta*, 2010, **411**, 1841-1848.

37. P. V. AshaRani, G. L. K. Mun, M. P. Hande and S. Valiyaveettil, *Acs Nano*, 2009, **3**, 279-290.

38. R. de Lima, A. B. Seabra and N. Duran, *Journal of Applied Toxicology*, 2012, **32**, 867-879.

39. T. Schatton, G. F. Murphy, N. Y. Frank, K. Yamaura, A. M. Waaga-Gasser, M. Gasser, Q. Zhan, S. Jordan, L. M. Duncan, C. Weishaupt, R. C. Fuhlbrigge, T. S. Kupper, M. H. Sayegh and M. H. Frank, *Nature*, 2008, **451**, 345-U311.

40. V. Stanic, D. Janackovic, S. Dimitrijevic, S. B. Tanaskovic, M. Mitric, M. S. Pavlovic, A. Krstic, D. Jovanovic and S. Raicevic, *Applied Surface Science*, 2011, **257**, 4510-4518.

41. A. Mishra, N. K. Kaushik, M. Sardar and D. Sahal, *Colloids and Surfaces B-Biointerfaces*, 2013, **111**, 713-718.

42. J. M. Zook, M. D. Halter, D. Cleveland and S. E. Long, *Journal of Nanoparticle Research*, 2012, **14**, 9.

43. Y. K. Chen, X. B. Zheng, Y. T. Xie, C. X. Ding, H. J. Ruan and C. Y. Fan, *Journal of Materials Science-Materials in Medicine*, 2008, **19**, 3603-3609.

44. M. Liong, B. France, K. A. Bradley and J. I. Zink, *Advanced Materials*, 2009, **21**, 1684-+.

45. I. Sondi and B. Salopek-Sondi, *Journal of Colloid and Interface Science*, 2004, **275**, 177-182.

46. J. A. Lemire, J. J. Harrison and R. J. Turner, *Nature Reviews Microbiology*, 2013, **11**, 371-384.

47. J. T. Zhang, X. L. Li, X. M. Sun and Y. D. Li, *Journal of Physical Chemistry B*, 2005, **109**, 12544-12548.

Synthesis of nanoparticles composed of silver and silver chloride for a plasmonic photocatalyst using an extract from a weed *Solidago altissima* (golden rod).

Abstract

Abstract

Phyto synthesis of nanomaterials is advantageous since it is economical, eco-friendly and simple and, what is more, in the synthetic protocols, non-toxic chemicals and biocompatible materials are used. Here, a green synthetic methodology of nanoparticles composed of silver and silver chloride (Ag@AgCl NPs) is developed using a leaf extract of *Solidago altissima* as a reducing agent. Utilisation of a terrestrial weed for the synthesis of Ag@AgCl NPs is a novel environmentally friendly approach considering that no toxic chemicals, external halide source or elaborate experimental procedures are included in the process. The optical properties and elemental compositions of as-synthesised Ag@AgCl NPs are well characterised and the degradation of an organic dye; i.e., Rhodamine B (RhB), is investigated using the Ag@AgCl NPs. We find that degradation of RhB is effectively achieved thanks to both surface plasmon resonance and semiconductor properties of Ag@AgCl NPs. The surface-enhanced Raman scattering and anti-bacterial activities are also examined.
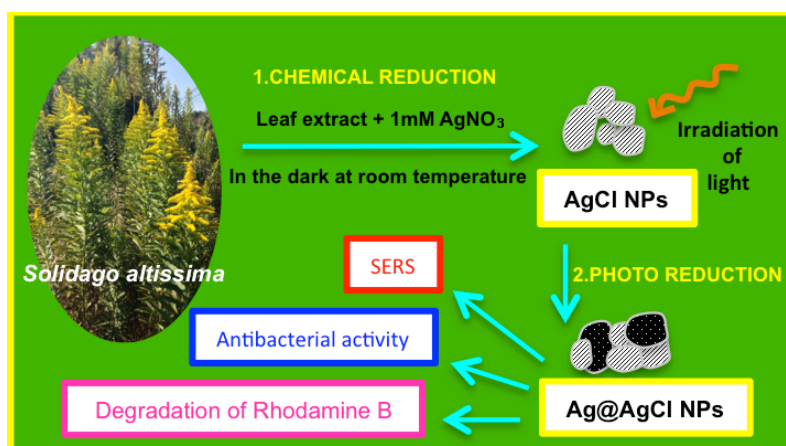
Introduction

3.1 Introduction

Weed species would in general cause hazardous situations on agricultural lands, which may eventually trigger loss of native biodiversity as well as serious economic damage [1] [2]. A terrestrial weed; *Solidago altissima*, belonging to the Asteraceae (Compositae) family, is commonly called golden rod. *S. altissima* is a native plant of North America and became a common alien plant in Japan several hundred years ago [3]. It is well known that *S. altissima* can grow in agricultural fields under various conditions, and the growth of rice seedlings, for example, can be seriously inhibited by *S. altissima*, which is mainly caused by allelo-chemicals such as 2-cis-dehydromatricaria ester (cis-DME) and methyl-10-(2-methyl-2-butenoyloxy)-2-cis-8-cis-decadiene-4,6-diynoate [4] [5], released from its rhizomes.

Phyto synthesis of nanomaterials would be advantageous in such a sense that it is economical, eco-friendly and simple and, what is more, in the synthetic protocols, non-toxic chemicals [6,7] and biocompatible [8] materials are used. Synthesis of metal nanoparticles using such green protocols is in great demand [9] since no toxic chemicals are emitted into the environment [10] and the synthetic devices can be easily scaled up since the procedures do not require any extreme conditions such as high pressure, energy and temperature. A variety of plant species have been used in the synthesis of nanoparticles [11] and it is known that Ag@AgCl NPs can also be phyto synthesised [12].

Ag@AgCl NPs were synthesised based on a green protocol using an extract of *S. altissima* for the first time. The structures and elements of the particles are well characterized and the photocatalytic activity of as-synthesized Ag@AgCl NPs is examined using Rhodamine B (RhB). We find that the degradation of RhB is effectively achieved thanks to both SPR and semiconductor properties of Ag@AgCl NPs. The surface enhanced Raman scattering (SERS) and anti-bacterial activities are also investigated. We suppose that the present approach to the synthesis of nanoparticles using a weed may encourage the utilisation of hazardous plants for the creation of novel nanomaterials, and that this may also help in the battle to conserve Nature.

Highlights:

- Aqueous leaf extract of a terrestrial weed was used in the synthesis and it acted as both reducing agent and halide supplement.
- Photo reduction during the synthesis has a notable influence on synthesis of Ag@AgCl NPs.
- Efficient photocatalytic performance.
- Antibacterial efficacy is quite high against both gram-negative and gram-positive bacteria.
- Particles showed a considerable SERS performance.

Experimental methods

3.2 Phyto synthesis of Ag-AgCl NPs

Fresh plant leaves of *S. altissima* were collected on the Kawagoe Campus, Toyo University, Japan and cleaned with millipore water to remove the surface contaminants. 10 g of leaf pieces were heated in 100 mL of millipore water at 90 ºC for 90 min, followed by filtration (Whatman Cat No 1002-185) to obtain an aqueous plant leaf extract. The leaf extract was refrigerated at 4 °C for further use. 20 mL of the aqueous leaf extract was mixed with 60 mL of 1 mM aqueous solution of silver nitrate ($AgNO_3$) (Sigma-Aldrich, Japan) at 4 °C, and the mixture was stirred for 30 min in the dark and then exposed to light (Power density: 1 sun = 100 mW cm^{-2}, Exposed area: 3 × 3 cm^2) (HAL 320, Asahi spectra Co., Ltd.) for 30 min. The mixture was centrifuged at 15000 rpm for 40 min to pelletize the product. The pellet was purified by dispersing it in millipore water, followed by centrifugation at 15000 rpm for 40 min.

Characterisation

3.3 Characterisation of Ag@AgCl NPs

The optical properties of as-synthesised NPs were characterized by an ultraviolet-visible-near infrared (UV-Vis-NIR) spectrophotometer (DU 730, Beckman Coulter) in the range from 200 to 1000 nm at a resolution of 1 nm, and a UV diffuse reflectance spectroscope (DH2000-DUV, USB2000, Ocean Optics Inc) in the range from 250 to 600 nm. The morphology of the particles was analyzed using a transmission electron microscope (TEM) (JEM2200FS, JEOL) at an acceleration voltage of 200 kV with a scan snap & orius camera and software (Gatan). Samples for TEM observation were prepared on a carbon coated copper grid (Cu 200 mesh, JEOL), dropping and drying nanoparticles' suspension on the grid. The elemental composition of the particles was analyzed by energy dispersive X-ray spectroscopy (EDS) (SU6600, Hitachi equipped with OXFORD X- Max^N). The crystal nature of the particles was determined by an X-ray diffractometer (XRD) (Smart Lab, Rigaku), using a Cu Kα X-ray of 0.154 nm wavelength supplied by a 9 kW rotating Cu anode X-ray generator, and employing a grazing-incidence X-ray diffraction geometry with a scanning diffraction angle (2θ) from 25° to 90° at 1.5° min^{-1} at an incident angle of 0.1°. The elemental and chemical bonding states of the nanoparticles were studied by an X-ray photoelectron spectroscope (XPS) (Axis-HIs, Kratos analytical) equipped with a non-monochromatic Al Kα X-ray of an energy of 1486.61 eV, pass energy of 80 eV and step energy of 0.1 eV at lower than 1.0×10^{-8} Torr. Samples for XPS were prepared on a hydro fluoric acid treated silicon wafer, dropping and drying nanoparticles' suspension on the wafer. The photo luminescence spectra (PL) of the particles were determined, using a spectrofluormeter (FP 6500, Jasco).

Characterisation of a leaf extract

The chemical functional groups of the organic compounds responsible for the reduction reaction were analysed by Fourier transform infrared spectroscopy (FT-IR) (Nicolet iS50, Thermo Fischer Scientific), scanning the IR from 400 to 4000 cm^{-1} at a resolution of 4 cm^{-1}. The leaf extract was centrifuged at 15000 rpm for 45 min, the supernatant was removed and the pellet was dried in vacuum. Samples for FT-IR measurement were prepared by the KBr pellet method [13]. The elemental composition of the leaf extract was analysed by EDS and XPS. Samples for EDS and XPS were prepared on a hydro fluoric acid treated silicon wafer, dropping and drying an aqueous leaf extract on the wafer.

Results
and
Discussion

3.4 Results and Discussion

Synthesis of Ag@AgCl NPs

Ag@AgCl NPs were successfully synthesised by the following two-step procedure; (1) The reduction of Ag^+ ($AgNO_3$) using an aqueous leaf extract of *S. altissima* to synthesise AgCl NPs, and (2) the photo reduction of AgCl NPs to synthesise Ag@AgCl NPs. The chemical compounds present in the aqueous leaf extract such as terpenoids [14], glycosides [15, 16], acetylenes [17, 18], phenols [3] and components containing chlorine (Cl^-) [19] were supposed to be responsible for the reduction reaction [20] [21] to synthesise AgCl NPs in the first procedure, noting that no external chlorine components or any additional chemicals were supplied during the synthesis (see **Figure 1** for FTIR, EDS and XPS analyses of the leaf extract). FTIR spectrum of a leaf extract is shown in **Figure 1(a)**. The peak positions corresponds to 3354.07 cm^{-1} (N-H, stretch), 2921.79 and 2851.17 cm^{-1} (C-H, stretch), 1640.75 cm^{-1} (N-H, bend), 1384.19 and 1327.46 cm^{-1} (S=O), 1156.92 and 1076.78 cm^{-1} (C-O), 781.52 cm^{-1} (C-Cl), 611.77 and 521.64 cm^{-1} (C-X) [22]. Note that the peak at 781.52 cm^{-1} represents chlorine related compounds. The EDS spectrum of a leaf extract is shown in **Figure 1(b)**. The peak positions represent phosphorous, sulfur and chlorine that were present in the leaf extract. The XPS data; i.e., the peaks of C1s, O1s and Cl2p, show that the present leaf extract was composed of some compounds bonded with carbon, oxygen and chlorine (**see Figure 1(c)**). **Figure 1(d)** shows two peaks corresponding to $Cl2p_{3/2}$ and $Cl2p_{1/2}$ centered at 198.29 and 199.95, which represent chorine related components are present in the leaf extract[23]. The peaks of C1s correspond to a binding energy of 284.6, 286.06, 293.09 and 295.72 eV (**see Figure 1(e)**).
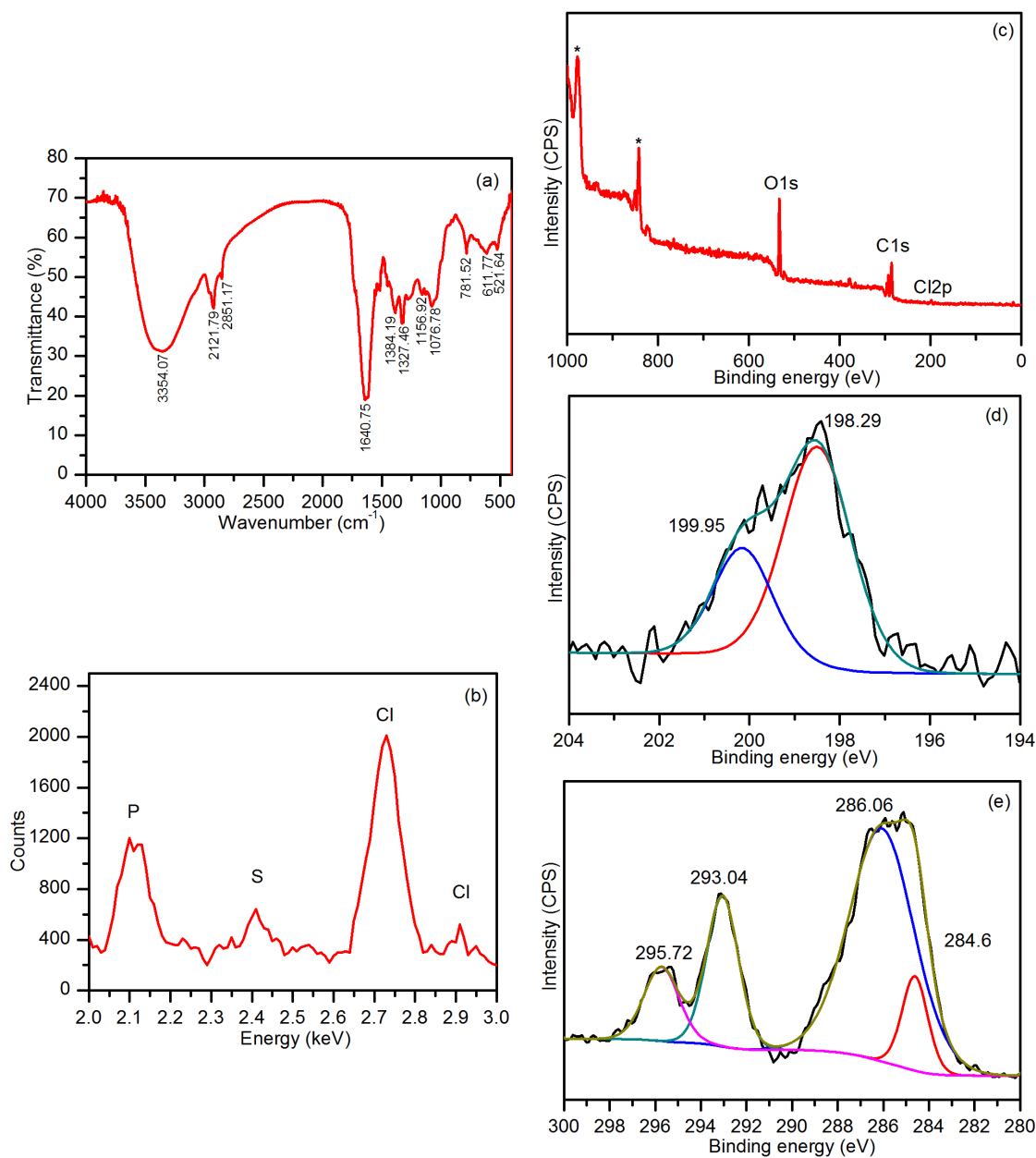
Figure 1. Characterisation of a leaf extract. (a) FTIR spectrum, (b) EDS spectrum, (c),(d),(e) XPS spectra.

The second procedure was performed by irradiation of light into the reaction mixture. Ag@AgCl NPs were synthesised owing to the high photosensitivity of AgCl [24] [25]. A pair of electron and hole are generated in AgCl via photon activation, and therefore it is supposed that the photogenerated electron promoted the conversion of Ag^+ ion into Ag^0 atom [25-27], resulting in the synthesis of Ag@AgCl NPs. The progress of the synthesis of Ag@AgCl NPs

was confirmed by the time variation of the UV-Vis-NIR spectrum of the reaction mixture during the synthetic procedure. As shown in **Figure 2**, the time variation of the peak intensity observed in the visible region depicts the gradual synthesis of Ag@AgCl NPs. **Figure 3** shows the UV-Vis-NIR spectrum of the purified Ag-AgCl NPs dispersed in millipore water, where the plasmonic resonance peak at 462 nm is attributed to Ag, whereas the absorption peak at 246 nm to AgCl [28]. The UV-Vis diffuse reflectance spectrum of dried Ag@AgCl NPs shows some absorbance in the visible light region due to surface plasmon resonance (SPR) in metallic Ag clusters in the powders [29], while the absorbance in the UV region is caused by AgCl NPs coupled with Ag NPs (see **Figure 4**) [30], which suggests that the present Ag@AgCl NPs can be used as an effective plasmonic photo catalyst in visible light [31].

UV-Vis-NIR Spectroscopy and UV-Vis diffuse reflectance spectroscopy
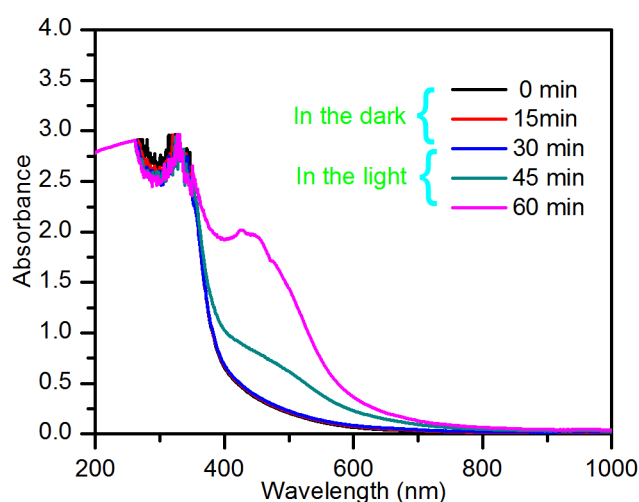
Figure 2. UV-Vis-NIR spectra of reaction mixture at regular intervals of time. The absorption peak at 462 nm increases gradually, representing the growth of Ag@AgCl NPs during the synthesis.
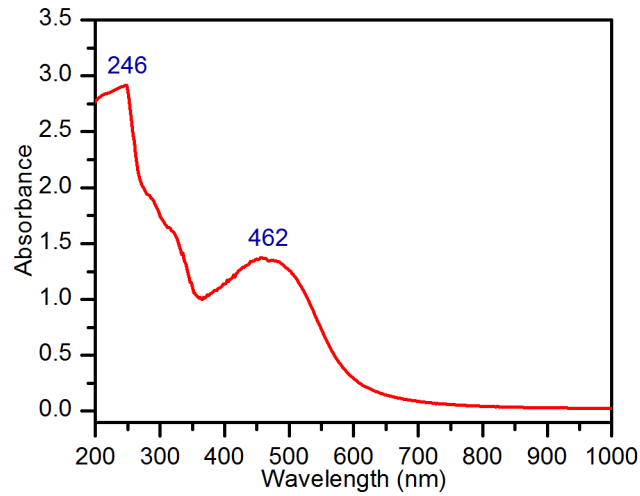
Figure 3. Absorption spectrum of purified Ag@AgCl NPs dispersed in millipore water.
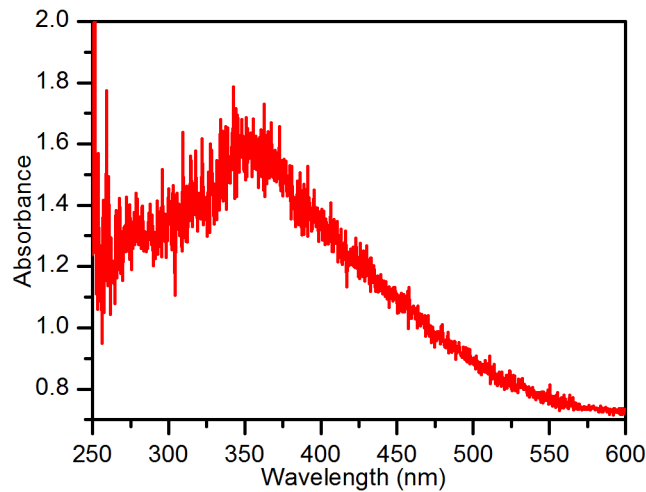
Figure 4. Absorption spectrum of dried Ag@AgCl NPs on a silicon substrate.

Spectroflourometery

The PL spectrum of the Ag@AgCl NPs at room temperature (24 ± 2 °C) showed emission bands at 318 and 470 nm when excited with photons of 200 nm wavelength, which also clarifies the semiconductor features of the present Ag@AgCl NPs (**Figure 5**).
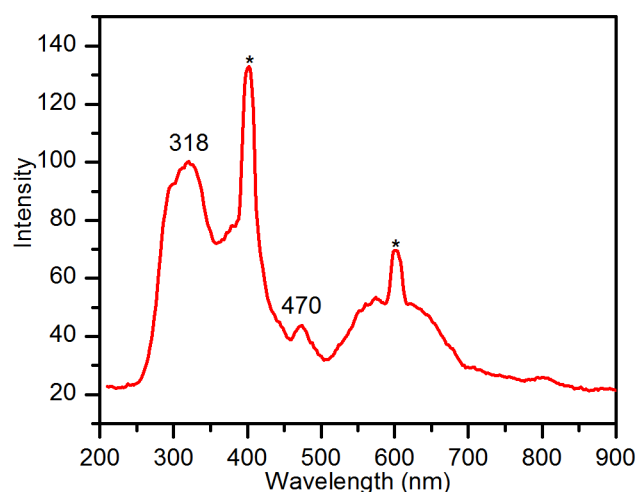
Figure 5. Photo luminescence spectrum of Ag@AgCl NPs. The emission peaks at 318 and 470 nm clarify the semi-conductor property of Ag@AgCl. The peaks indicated by asterisks are caused by higher-order diffraction.

X-ray diffraction, Transmission electron microscopy, scanning electron microscopy and energy dispersive X-ray spectroscopy

The morphology and crystalline nature of the particles were investigated by SEM, EDS, TEM and XRD. SEM, EDS, TEM and FFT images of the particles are shown in **Figure 6**. A large number of clusters of particles, which were composed of Ag and Cl, were produced (**Figure 7(a)** and **7(b)**). It is clearly shown that each cluster was composed of Ag and AgCl (**Figure 7(c), 7(d), 7(e) and 7(f)**), noting that the lattice fringe distance of 0.23 nm corresponds to Ag (111), whereas 0.27 nm to AgCl (200) (**Figure 7(d), 7(e)** and **7(f)**). The peaks in the diffractogram also confirm the cubic AgCl and cubic Ag structures, respectively, with the lattice constant 5.553050 Å (ICDD 01-071-5209) and 4.097667 Å (ICDD 00-041-1402) (**Figure 6**).
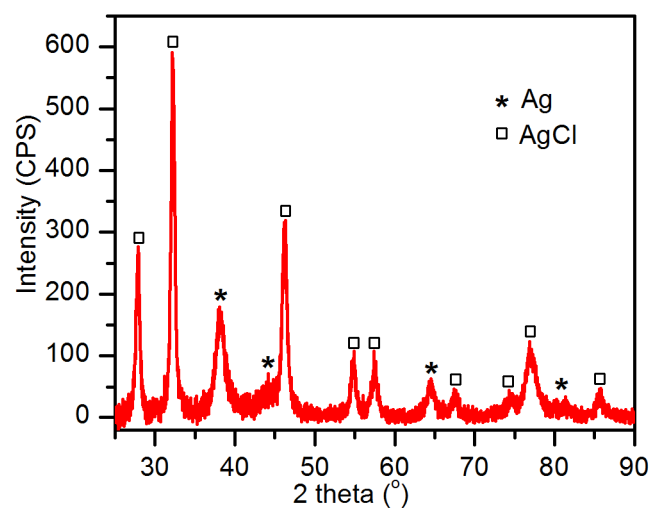
Figure 6. X-ray diffractogram of as-synthesised nanoparticles. The data also confirms that the clusters are composed of Ag and AgCl.
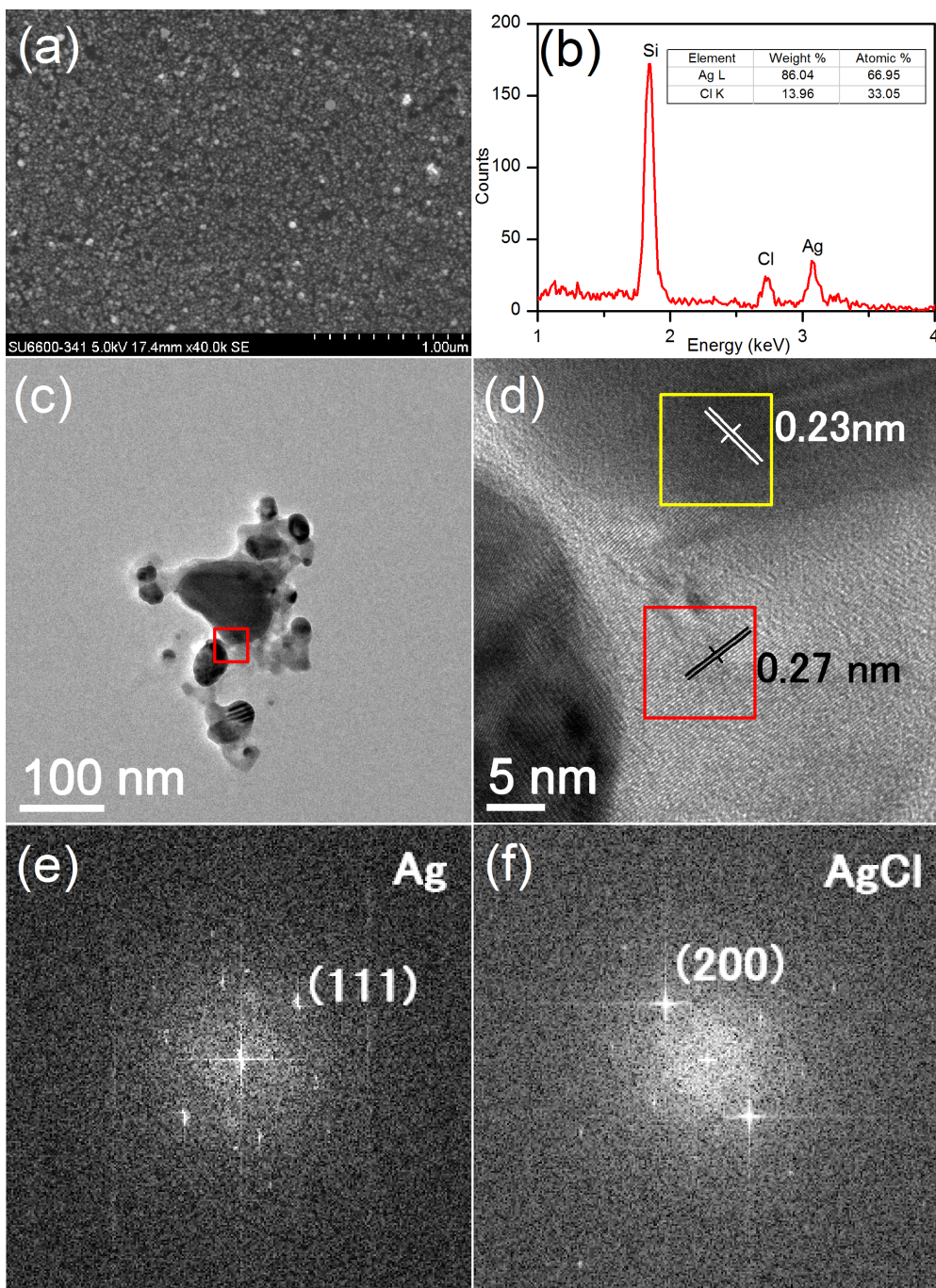
Figure 7. SEM, EDS, TEM and FFT images of Ag@AgCl NPs. (a) SEM image of clusters of nanoparticle; (b) EDS spectrum of Ag@AgCl NPs, inset showing atomic and weight percentages of silver and chlorine; (c) TEM image of a cluster; (d) TEM image of the region represented by red square in image (c). The gaps between two neighbouring fringes are 0.23 and 0.27 nm, which, respectively, coincide with those of silver (111) and silver chloride (200); (e),(f) FFT images of the regions represented by yellow and red squares in image (d). It is clearly shown that each cluster is composed of Ag and AgCl.

X-ray photoelectron spectroscopy

The elemental composition of the as-synthesised nanoparticles was analysed by XPS. The wide scan spectrum indicates the presence of Ag, Cl, C and O (**Figure 8(a)**). Ag 3d $_{5/2}$ and Ag 3d $_{3/2}$ centered at 367.75 and 373.76 eV represent AgCl [32, 33] (**Figure 8(b)**), whereas Cl 2p $_{3/2}$ and Cl 2p $_{1/2}$ centered at 197.90 and 199.57 eV represent Ag@AgCl NPs [23] [34] (**Figure 8(c)**).
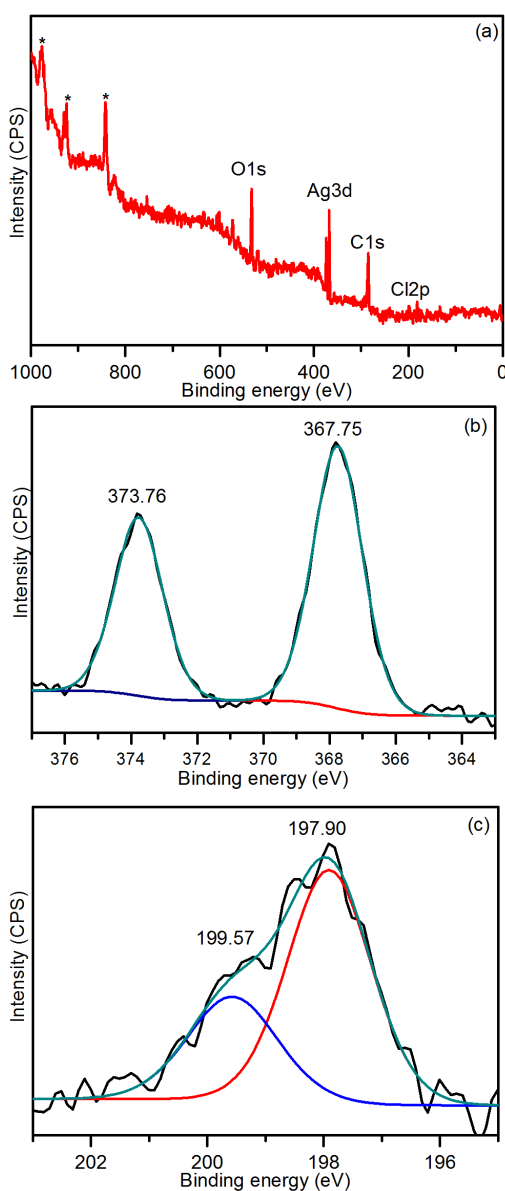

Figure 8. XPS spectra of as-synthesised particles. (a) Wide scan spectrum. The peaks indicated by asterisks represent unassigned Auger ones ; (b) Ag3d; (c) Cl2p.

Photo catalytic performance of Ag@AgCl NPs

2 mg of nanoparticles were mixed with 2 mL of 10 mg L^{-1} aqueous solution of Rhodamine B (RhB) (Tokyo chemical industry co., Ltd) for 30 min in the dark for the establishment of adsorption/desorption equilibrium of RhB on the particles. Then, the mixture was transferred to a quartz photo-reactor for the measurement of the photo catalytic activity of the nanoparticles. The photo-reactor was irradiated with light from a solar simulator without any cutoff filters (Power density: 1 sun = 100 mW cm^{-2}, Exposed area 3 × 3 cm^2) (HAL 320, Asahi Spectra Co., Ltd.) ranging from 350 to 1100 nm to evaluate the degradation of RhB. Aliquots of the reaction mixture were collected and centrifuged at 15000 rpm for 10 min to separate the photo catalyst from the mixture and UV-Vis-NIR absorption by the supernatant was recorded by the UV-Vis-NIR spectrophotometer from 0 to 60 min at regular intervals of time to measure the degradation of RhB. Degraded RhB was further confirmed by a mass spectroscope (MS) (amaZon speed, Brüker Daltonics) by the direct probe method, using an atmospheric pressure chemical ionization (APCI) source at the mass-to-charge ratio (m/z) ranging from 15 to 600 amu. For examining the enhancement of the photocatalytic efficiency of the present nanoparticles, another experiment was carried out using a commercialized photo catalyst Ag$_3$PO$_4$, the average size of which was 25 to 600 nm (Sigma-Aldrich, Japan), under the same experimental conditions. RhB molecules in aqueous solution show three major peaks at 258, 354 and 554 nm in the UV-Vis absorption spectrum. **Figure 9(a)** and **9(b)** show the time variations of the absorption spectra in the presence of Ag@AgCl and Ag$_3$PO$_4$. The decrease in the peak intensity and the shift of the peak position towards lower energy regions elucidate the degradation of RhB molecules and N-deethylation [35]. The photo catalytic activity was evaluated by the UV-Vis absorption at 554 nm. The time variation of - ln (C/C_0), where C is the concentration of the dye at regular intervals of time t, and C_0 the concentration at $t = 0$, is shown in **Figure 9(c)**. The rate constant k for the degradation reaction of RhB based on the first order reaction kinetics (ln (C/C_0) = - k t) is calculated to be 0.0387 min^{-1} in the case of Ag@AgCl NPs, whereas k = 0.0237 min^{-1} in the case of Ag$_3$PO$_4$. The high

photocatalytic performance of Ag@AgCl NPs owes to the SPR of Ag NPs and the semiconductor features of AgCl NPs [36] [33]. A further confirmation of the degradation of RhB by Ag@AgCl was carried out by mass spectrometric analysis. **Figure 10** shows the peaks at 442, 413, 386, 357 and 329 m/z, which correspond to RhB and its N-deethylated intermediates [37]. It is clearly shown that the degradation of RhB is encouraged by the present Ag@AgCl.
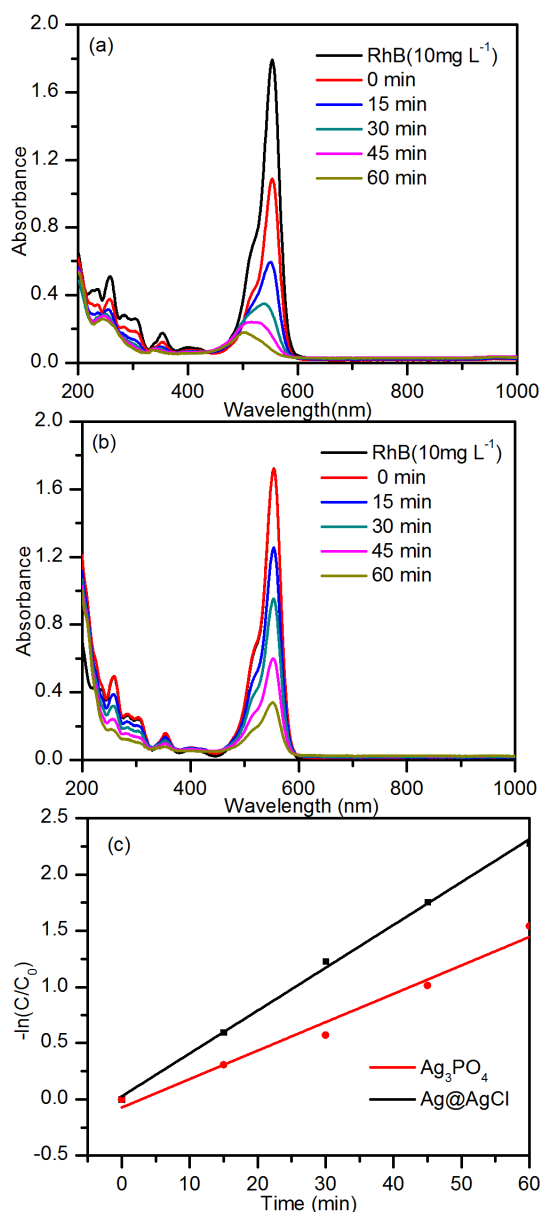

Figure 9. Degradation of RhB. (a) UV-Vis-NIR absorption spectrum of RhB degraded by Ag@AgCl NPs at regular intervals of time; (b) UV-Vis-NIR absorption spectrum of RhB degraded by Ag_3PO_4 NPs; (c) Time variation of $-\ln(C/C_0)$, where C is the concentration of the dye at time t and C_0 the concentration at $t = 0$.
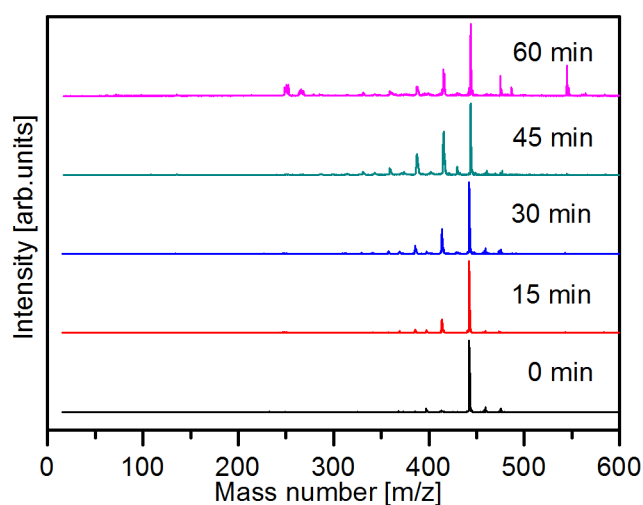
Figure 10. Mass spectra of RhB degraded by Ag@AgCl NPs at regular time intervals.

The change in the ratio of Ag and AgCl in the Ag@AgCl NPs before and after the photocatalytic experiment was evaluated by XRD analysis (**Figure 11**). The peak intensities in the XRD spectrum and weight percentages of Ag and AgCl changed quite significantly after the experiment due to the photosensitivity of AgCl, noting that no cut-off filter was used during light irradiation in the present study. The previous studies showed that Ag NPs on the AgCl NPs were structurally stable and catalytically reusable thanks to the cut-off filter of UV light [27] [38] and therefore we believe that the catalytic performance of the present Ag@AgCl will be improved by introducing the cut-off filter of UV light.
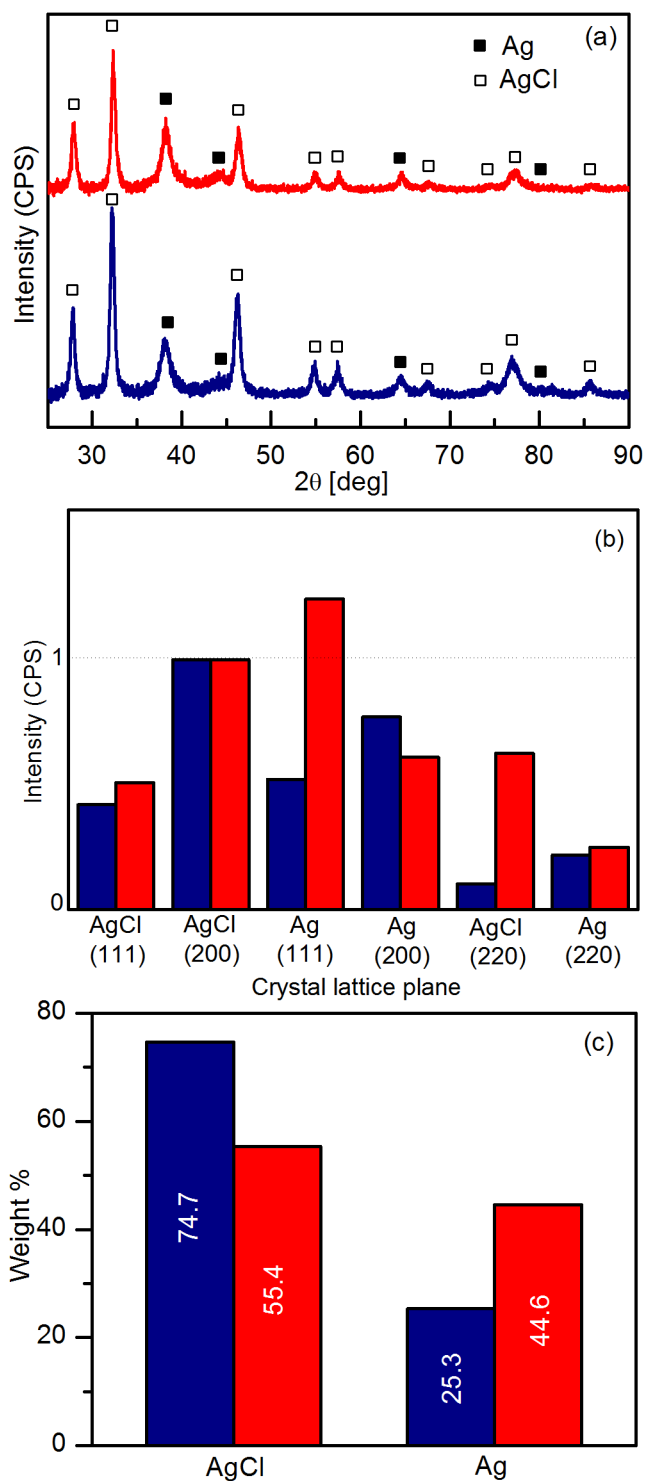
Figure 11. XRD analysis of Ag@AgCl NPs before and after the photo catalysis experiment (a) X- ray diffractogram of Ag@AgCl NPs before (blue) and after the experiment (red); (b) Intensities at different peak positions, representing various crystal lattice planes of diffractogram of Ag and AgCl before (blue) and after the experiment (red); (c) Weight percentages of AgCl and Ag before (blue) and after the experiment (red).

SERS activity of Ag@AgCl NPs

The SERS characteristics were investigated using an aqueous solution of RhB. 0.1 mM RhB solution was dropped onto dried Ag@AgCl NPs placed on a glass substrate and the Raman spectra were obtained using a micro-Raman spectroscopic system (Lab Ram HR800UV, Horiba Jobin Yvon S.A.S.) with an excitation wavelength of 633 nm. The spot diameter and power of the laser beam were, respectively, 2 µm and 43.6 µW and the spectra were obtained with a 5-sec integration. Raman spectra of an aqueous solution of RhB, which was dropped onto Ag@AgCl NPs placed on a glass substrate, was obtained (**Figure 12**). It is clearly shown that Raman signals were greatly enhanced in the presence of Ag@AgCl NPs, noting that each peak coincides with that of rhodamine B [39] and therefore the present Ag@AgCl NPs are highly SERS active thanks to Ag NPs [40] [41], whereas there were no recognisable signals of rhodamine B when the solution was dropped onto the surface of a glass substrate.
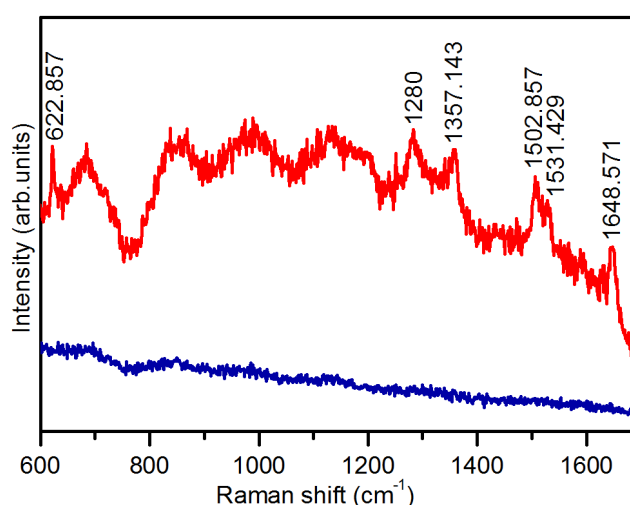
Figure 12. Raman spectra of 0.1 mmol aqueous solution of RhB. The red curve represents a Raman spectrum of RhB solution dropped on dried Ag@AgCl NPs, whereas the blue curve the spectrum of the solution dropped on a glass substrate. The Raman spectrum of RhB on Ag@AgCl NPs shows several sharp peaks, which are typical ones of RhB molecules.

Antibacterial activity

To examine the antibacterial activity of the Ag@AgCl NPs, the time variation of the bacterial growth was measured for 15 h, culturing two bacterial species; *Escherichia coli* (Gram-negative) and *Bacillus subtilis* (Gram-positive) in Nutrient broth No.2 (Oxoid) media supplemented with an aqueous solution of Ag@AgCl NPs, the concentration of which was changed; 5, 10 and 20 µg mL^{-1}, at 37 °C under a constant shaking at 150 rpm. The optical density (O.D) values at 600 nm were recorded every 30 min using an OD-Monitor (C&T, Taitec Corp.). The growth of *Escherichia coli* and *Bacillus subtilis* in the presence of Ag@AgCl NPs was reduced even when the concentration of Ag@AgCl NPs was as low as 5 µg mL^{-1}.[42][43] (**Figure 13**).
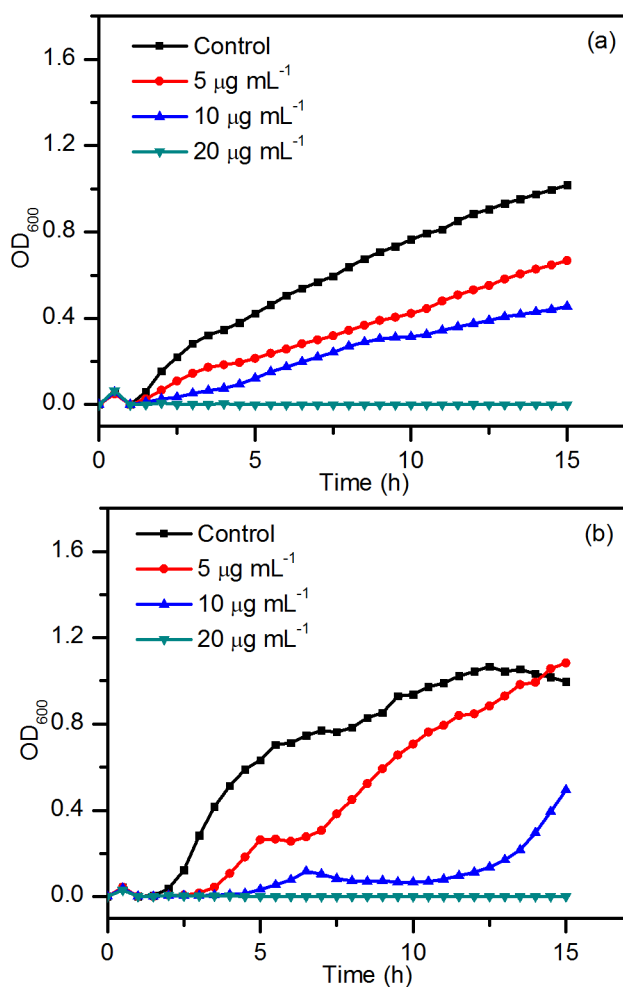
Figure 13. Time variations of the growth of *Escherichia coli* and *Bacillus subtilis* in the presence of Ag@AgCl NPs.

Conclusion

3.5 Conclusions

A green method was developed for synthesising an effective plasmonic photocatalyst based on two-step procedure; i.e., (1) Production of AgCl NPs via the reduction of Ag+ ($AgNO_3$) using an aqueous leaf extract of *S. altissima,* and (2) Production of Ag@AgCl NPs via the photo reduction of AgCl NPs. The optical properties and elemental compositions of as-synthesised Ag@AgCl NPs were well characterised. We found that degradation of RhB was effectively achieved thanks to both surface plasmon resonance and semiconductor properties of Ag@AgCl NPs. The particles also showed high surface-enhanced Raman scattering and anti-bacterial activities. The present green approach to the synthesis of nanoparticles using a weed may encourage the utilisation of hazardous plants for the creation of novel nanomaterials.

References

References

1. http://www.niaes.affrc.go.jp/techdoc/apasd/Solidago%20altissima%20-B.html

2. https://rsis.ramsar.org/ris/2057

3. H. Jin, T. Tanaka, I. Kouno and K. Ishimaru, *Journal of Natural Medicines*, 2007, **61**, 351-354.

4. Kawazu K, Nakamura A, Nishino C, Koshimizu K, Mituii T, Tokyo, 1969.

5. K. Ichihara, T. K, M. Kaji and M. Noda, *Agriculture and Biological chemistry*, 1976, **40**, 353-358.

6. P. Raveendran, J. Fu and S. L. Wallen, *Journal of the American Chemical Society*, 2003, **125**, 13940-13941.

7. J. M. DeSimone, *Science*, 2002, **297**, 799-803.

8. V. K. Sharma, R. A. Yngard and Y. Lin, *Advances in Colloid and Interface Science*, 2009, **145**, 83-96.

9. S. Iravani, *Green Chemistry*, 2011, **13**, 2638-2650.

10. S. P. Dubey, M. Lahtinen and M. Sillanpaa, *Colloids and Surfaces a-Physicochemical and Engineering Aspects*, 2010, **364**, 34-41.

11. S. K. Srivastava, C. Ogino, A. Kondo in *Green Processes for Nanotechnology*, ed. E. V. B. Vladimir A. Basiuk, Springer International Publishing, 2015, ch. 8, pp. 237-257.

12. A. A. Kulkarni and B. M. Bhanage, *ACS Sustainable Chemistry & Engineering*, 2014, **2**, 1007-1013.

13. N. B. Colthup, L. H. Daly and S. E. Wiberley, *Introduction to Infrared and Raman Spectroscopy*, Academic press, New york-London, 1964.

14. A. T. Merritt and S. V. Ley, *Natural Product Reports*, 1992, **9**, 243-287.

15. B. Wu, T. Takahashi, T. Kashiwagi, S. I. Tebayashi and C. S. Kim, *Chemical & Pharmaceutical Bulletin*, 2007, **55**, 815-816.

16. H. Jin, K. Ogino, T. Fujioka, M. Yoshida and K. Ishimaru, *Journal of Natural Medicines*, 2008, **62**, 199-201.

17. A. Kobayashi, S. Morimoto, Y. Shibata, K. Yamashita and M. Numata, *Journal of Chemical Ecology*, 1980, **6**, 119-131.

18.   A. Okano, Y. Nomura and **T.** Tezuka, *Journal of natural products*, 1983, **46**, 750-751.

19.   K. C. Engvild, *Phytochemistry*, 1986, **25**, 781-791.

20.   K. B. Narayanan and N. Sakthivel, *Materials Research Bulletin*, 2011, **46**, 1708-1713.

21.   C. A. Rice-Evans, N. J. Miller and G. Paganga, *Free Radical Biology and Medicine*, 1996, **20**, 933-956.

22.   D. L.Pavia, G. M.Lampman, G. S.Kriz and J. R.Vyvyan, *Introduction to spectroscopy*, Brooks/Cole, USA, 4 edn., 2009.

23.   C. D.Wagner, W. M. Riggs, L. E. Davis, J. F. Moulder and G. E. Muilenburg, *Handbook of X-ray Photoelectron Spectroscopy*, Perkin-Elmer Corp., Physical Electronics Division: Eden Prairie, Minnesota, 1979.

24.   X. C. Ma, Y. Dai, L. Yu, Z. Z. Lou, B. B. Huang and M. H. Whangbo, *Journal of Physical Chemistry C*, 2014, **118**, 12133-12140.

25.   G. Wang, T. Nishio, M. Sato, A. Ishikawa, K. Nambara, K. Nagakawa, Y. Matsuo, K. Niikura and K. Ijiro, *Chemical Communications*, 2011, **47**, 9426-9428.

26.   M. M. Husein, E. Rodil and J. H. Vera, *Journal of Colloid and Interface Science*, 2005, **288**, 457-467.

27.   P. Wang, B. B. Huang, X. Y. Qin, X. Y. Zhang, Y. Dai, J. Y. Wei and M. H. Whangbo, *Angewandte Chemie-International Edition*, 2008, **47**, 7931-7933.

28.   J. G. McEvoy and Z. S. Zhang, *Applied Catalysis B-Environmental*, 2014, **160**, 267-278.

29.   J. Jiang and L. Z. Zhang, *Chemistry-a European Journal*, 2011, **17**, 3710-3717.

30.   H. Lei, W. Ping, Z. Chengzhou, Z. Yueming and D. Shaojun, *Nanoscale*, 2011, **3**, 2931-2935.

31.   P. Wang, B. B. Huang, Z. Z. Lou, X. Y. Zhang, X. Y. Qin, Y. Dai, Z. K. Zheng and X. N. Wang, *Chemistry-a European Journal*, 2010, **16**, 538-544.

32. H. Zhang, G. Wang, D. Chen, X. J. Lv and U. H. Jinghong, *Chemistry of Materials*, 2008, **20**, 6543-6549.

33. R. F. Dong, B. Z. Tian, C. Y. Zeng, T. Y. Li, T. T. Wang and J. L. Zhang, *Journal of Physical Chemistry C*, 2013, **117**, 213-220.

34. D. L. Chen, S. H. Yoo, Q. S. Huang, G. Ali and S. O. Cho, *Chemistry-a European Journal*, 2012, **18**, 5192-5200.

35. S. N. Zhang, H. F. Tian, S. J. Zhang, L. M. Song, X. Q. Wu, J. Y. Ye and Q. W. Wei, *Chemical Engineering Journal*, 2014, **240**, 548-553.

36. Z. Y. Lin, J. Xiao, J. H. Yan, P. Liu, L. H. Li and G. W. Yang, *Journal of Materials Chemistry A*, 2015, **3**, 7649-7658.

37. K. Yu, S. G. Yang, H. He, C. Sun, C. G. Gu and Y. M. Ju, *Journal of Physical Chemistry A*, 2009, **113**, 10024-10032.

38. C. H. An, S. N. Peng and Y. G. Sun, *Advanced Materials*, 2010, **22**, 2570-2574.

39. X. M. Qian, X. H. Peng, D. O. Ansari, Q. Yin-Goen, G. Z. Chen, D. M. Shin, L. Yang, A. N. Young, M. D. Wang and S. M. Nie, *Nature Biotechnology*, 2008, **26**, 83-90.

40. Y. Yang, S. Matsubara, L. M. Xiong, T. Hayakawa and M. Nogami, *Journal of Physical Chemistry C*, 2007, **111**, 9095-9104.

41. J. T. Zhang, X. L. Li, X. M. Sun and Y. D. Li, *Journal of Physical Chemistry B*, 2005, **109**, 12544-12548.

42. I. Sondi and B. Salopek-Sondi, *Journal of Colloid and Interface Science*, 2004, **275**, 177-182.

43. J. A. Lemire, J. J. Harrison and R. J. Turner, *Nature Reviews Microbiology*, 2013, **11**, 371-384.

Chapter 4

Synthesis of nanoparticles composed of silver and silver chloride for a plasmonic photocatalyst using an extract from needles of *Pinus densiflora*

Abstract

ABSTRACT

Nanoparticles composed of silver and silver chloride (Ag@AgCl NPs) are synthesised by a two-step procedure; (1) Synthesis of silver chloride nanoparticles (AgCl NPs) via phyto reduction mixing an aqueous extract from needles of *Pinus densiflora* (red pine) with an aqueous solution of silver nitrate ($AgNO_3$) in the absence of light; and (2) synthesis of Ag@AgCl NPs via photo reduction exposing AgCl NPs to light. The optical properties and elemental composition of as-synthesised Ag@AgCl NPs are examined for further applications of the nanoparticles as a plasmonic photocatalyst.
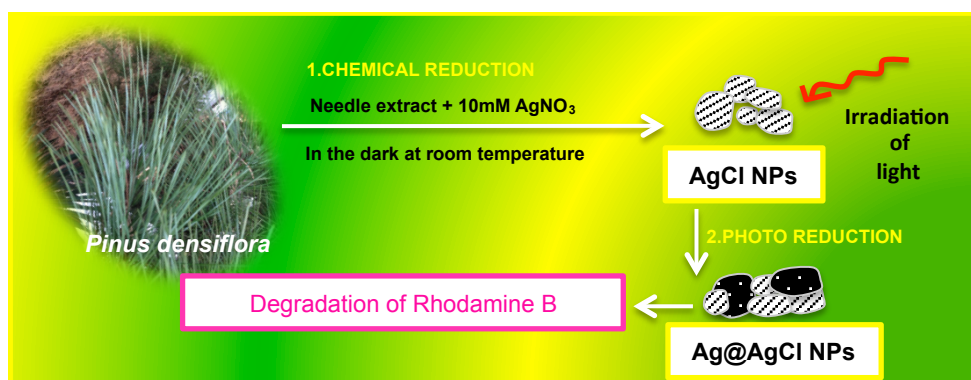
Introduction

4.1 Introduction

Nanoparticles composed of silver and silver chloride (Ag@AgCl NPs) have been drawn a lot of attention thanks to their high photocatalytic activity in the degradation of organic dyes [1] [2]. Silver chloride nanoparticles (AgCl NPs), which are a photosensitive semiconductor with a direct bandgap of 5.15 eV and indirect bandgap of 3.25 eV [3], possess notable electronic, magnetic, optical and catalytic properties [4], Silver nanoparticles (Ag NPs), which are one of the noble metallic particles, have a high scattering and enhancement characteristics of visible light due to the surface plasmon resonance (SPR) effect [5]. Ag NPs coupled with AgCl NPs (Ag@AgCl NPs) can therefore be used as an effective photocatalyst owing to the SPR characteristics of Ag NPs and semiconductor properties of AgCl NPs [6]. Several methods such as the hydrothermal method [7], *in-situ* anion exchange method[8] and *in-situ* photoactive method [9] have been developed to synthesise Ag@AgCl NPs, but some toxic chemicals, external halide sources and additional stabilising agents are required in the synthetic procedure and the reaction time is rather long. Therefore, it is still necessary to develop an eco-friendly method for synthesising photocatalytic nanoparticles. Here, a green method for synthesising Ag@AgCl NPs utilising an aqueous extract from needles of *Pinus densiflora* as a reducing agent is developed. The photocatalytic efficiency of as-synthesised Ag@AgCl NPs is examined, evaluating the degradation of Rhodamine B (RhB).

Highlights

- Nanoparticles composed of silver and silver chloride (Ag@AgCl NPs) are synthesised using an aqueous extract from needles of *Pinus densiflora*.
- Neither external chemicals nor halide sources are used in the synthetic protocol.
- Ag@AgCl NPs act as an effective plasmonic photocatalyst.

Experimental methods

4.2 Methodology

Fresh needles of P. densiflora were collected on the Kawagoe Campus, Toyo University, Japan and cleaned with milli-Q water to remove the surface contaminants. 10 g of needles with 100 mL of milli-Q water were autoclaved at 121 ºC for 15 min, followed by filtration (Whatman Cat No 1002-185) to obtain an aqueous solution of an extract from the needles. 10 mL of the solution was mixed with 30 mL of 10 mM aqueous solution of silver nitrate ($AgNO_3$) (Sigma-Aldrich, Japan), and the mixture was stirred for 30 min in the dark and then exposed to light from a solar simulator (Power density: 100 mW cm^{-2}, Exposed area: 3 × 3 cm^2) (HAL 320, Asahi spectra Co., Ltd.) for 10 min. The reaction mixture was centrifuged at 15000 rpm for 60 min to collect particles. The particles were purified by dispersing them in milli-Q water, followed by centrifugation at 15000 rpm for 60 min.

Characterisation

4.3 Characterization of Ag@AgCl NPs

The optical properties of as-synthesised NPs were characterised by a UV-Vis-NIR spectrophotometer (DU 730, Beckman coulter). The morphology of the nanoparticles was analysed using a transmission electron microscope (TEM) (JEM2200FS, JEOL) and scanning electron microscope (SEM) (SU6600, HITACHI). The elemental composition of the particles and extract from the needles was analysed by energy dispersive X-ray spectroscopy (EDS) (SU6600, HITACHI equipped with OXFORD, X-Max^N). The crystal nature of the particles was determined by an X-ray diffractometer (XRD) (Smart Lab, Rigaku). The elemental and chemical bonding states of the nanoparticles and extract from the needles were studied by an X-ray photoelectron spectroscope (XPS) (Axis-HIs, Kratos analytical) equipped with a non-monochromatic Mg Kα X-ray.

Results
and
Discussion

4.4 Results and discussion

Ag@AgCl NPs were successfully synthesised via the two-step procedure; (i) The reduction of Ag^+ ions using an aqueous extract from needles of *P. densiflora* to synthesise AgCl NPs, and (ii) the photo reduction of AgCl NPs to synthesise Ag@AgCl NPs. The chemical compounds present in the aqueous extract from the needles such as terpenoids, flavonoids, phenols, proanthocyanidin and components containing chlorine (Cl^-) [10] [11] [12] were supposed to be responsible for the reduction reaction [13] [14] to synthesise AgCl NPs in the first procedure, noting that neither external chlorine components nor additional chemicals were supplied during the synthetic procedure. (**Figure 1(a)**) shows the EDS spectra of an extract from needles of *Pinus densiflora*. The chemical components were composed of phosphorous, sulphur, chlorine and potassium. The chlorine present in the extract from the needles assisted the synthesis of AgCl NPs as a halide source in the first procedure. **Figure 1(b)** and **1(c)** shows the XPS spectra of Cl2p, which also clarifies the existence of chlorine. The second procedure was performed by irradiation of light into the reaction mixture. Ag@AgCl NPs were synthesised owing to the high photosensitivity of AgCl [15] [16]. It is supposed that a pair of electron and hole were generated in AgCl via photon activation, and consequently the photogenerated electron promoted the conversion of Ag^+ ion into Ag^0 atom [16, 17, 18], resulting in the formation of Ag@AgCl NPs.
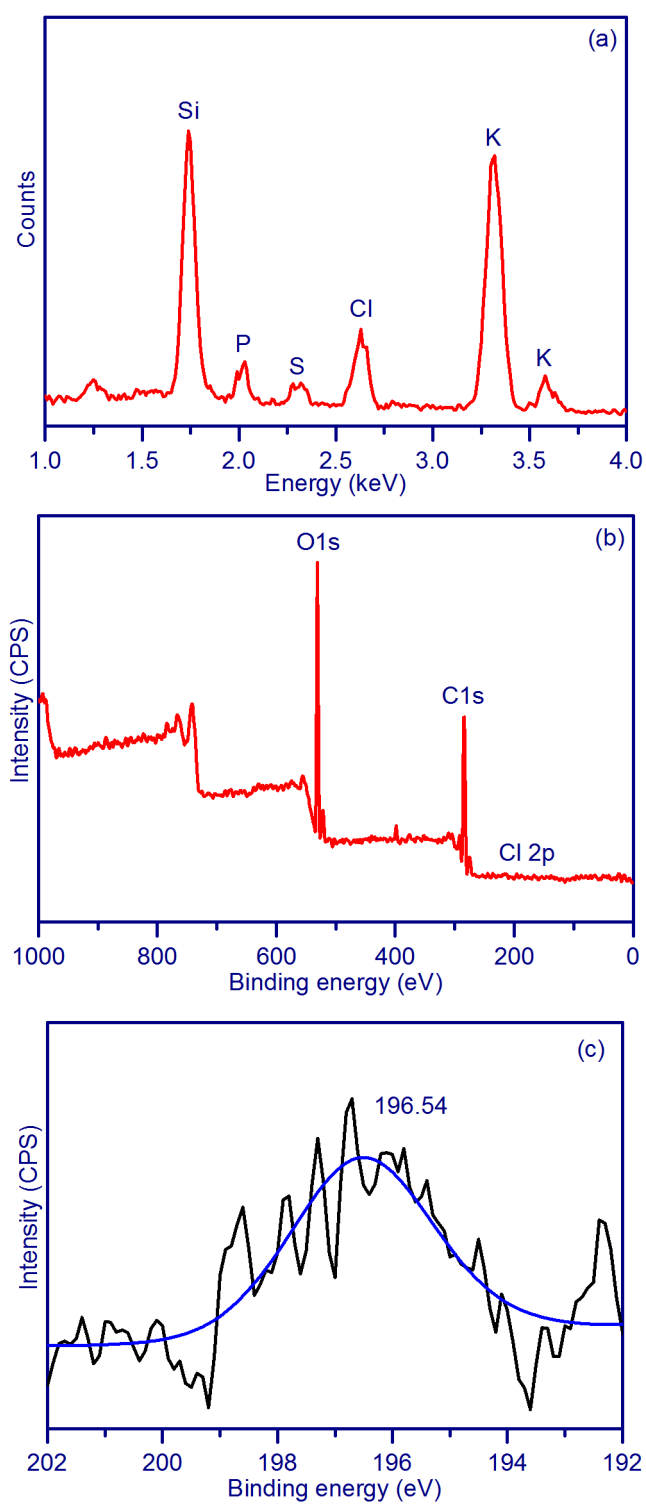
Figure 1. Characterisation of an extract from needles of *Pinus densiflora*. (a) EDS spectrum. The Si signal is from the substrate; (b) XPS wide scan spectrum; (c) Cl2p.

The synthesis of Ag@AgCl NPs was primarily confirmed by the time variation of the UV-Vis-NIR absorption spectrum of the reaction mixture during the synthetic procedure. As shown in **Figure 2** in the Supplementary data, the peak intensity observed in the visible region depicts the synthesis of Ag@AgCl NPs. **Figure 3** shows the UV-Vis-NIR spectrum of the purified Ag@AgCl NPs dispersed in milli-Q water, where the plasmonic resonance peak at 438 nm is assigned to Ag, whereas the absorption peak at 263 nm to AgCl [19].
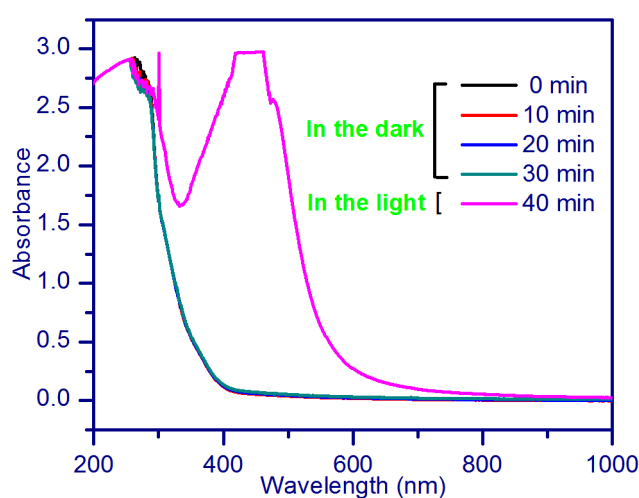
Figure 2. UV-Vis-NIR spectra of a reaction mixture at regular intervals of time. The absorption peak at 438 nm represents the growth of Ag@AgCl NPs during the synthesis. Note that the peak intensity reached the unmeasurable range of the UV-Vis-NIR spectrophotometer at 40 min.
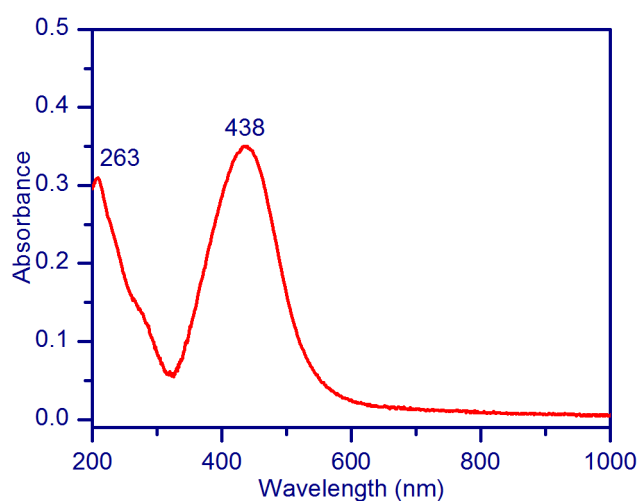
Figure 3. Absorption spectrum of purified Ag@AgCl NPs dispersed in milli-Q water. Peaks at 263 and 438 nm are, respectively, attributed to AgCl and Ag.

The morphology and crystalline nature of the particles were investigated by SEM, EDS, TEM and FFT images and XRD diffractogram (**Figure 4**). A large number of clusters of particles, which were composed of Ag and Cl, were synthesised (**Figure 4(a) and 4(b)**). It is clearly shown that each cluster was composed of Ag and AgCl, noting that the FFT images correspond to AgCl (200) and Ag (200) (**Figure 4(c), 4(d) and 4(e)**). The peaks in the X-ray diffractogram also confirm cubic AgCl and cubic Ag structures, respectively, with the lattice constant 5.540486 Å (ICDD 01-071-5209) and 4.090305 Å (ICDD 01-071-4613) (**Figure 4(f)**).
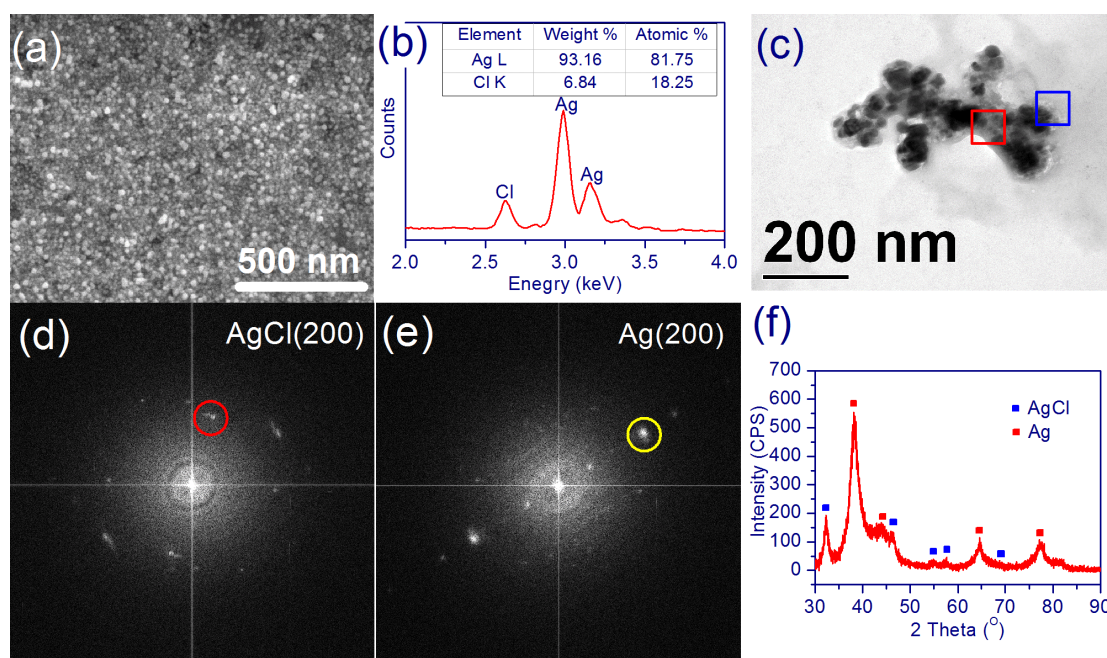
Figure 4. SEM, EDS, TEM and FFT images and XRD difractogram of Ag@AgCl NPs. (a) SEM image of clusters of nanoparticles; (b) EDS of clusters of nanoparticles, inset showing the atomic and weight percentages of silver and chlorine; (c) TEM image of a cluster composed of Ag and AgCl NPs; (d) FFT image of AgCl (200) (red circle) corresponding to the region indicated by red square on the TEM image (c); (e) FFT image of Ag (200) (yellow circle) corresponding to the region indicate by blue square on the TEM image (c); (f) X-ray diffractogram of Ag@AgCl NPs, representing the peaks of AgCl and Ag.

The elemental composition of as-synthesised nanoparticles was analysed by XPS (**Figure 5**). The wide scan spectrum indicates the presence of Ag, Cl, C and O (**Figure 5(a)**). $Ag3d_{5/2}$ and $Ag3d_{3/2}$ centred at 374.34 and 368.34 eV are attributed to metallic Ag^0, whereas those centred at 373.34 and

367.35 eV to Ag$^+$ in AgCl (**Figure 5(b)**) [20]. Cl2p centred at 197.79 eV represents the chlorine present in Ag@AgCl NPs (**Figure 5(c)**) [21][22].
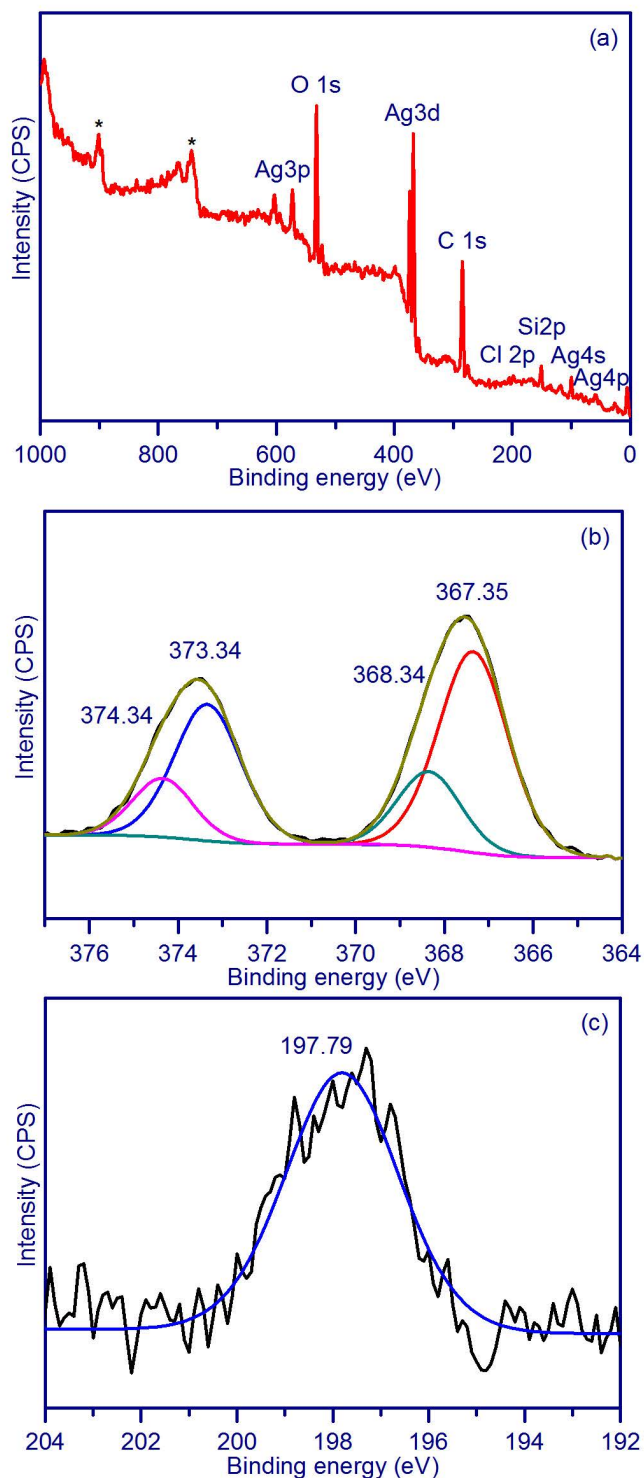

Figure 5. XPS spectra of as-synthesised particles. (a) Wide scan spectrum. The peaks indicated by asterisks represent unassigned Auger ones; (b) Ag3d; (c) Cl2p.

Measurement of the photocatalytic activity

2 mg of nanoparticles were mixed with 2 mL of 10 mg L^{-1} aqueous solution of Rhodamine B (RhB) (Tokyo chemical industry co., Ltd) for 30 min in the dark for the establishment of adsorption/desorption equilibrium of RhB on the particles. Then, the mixture was transferred to a quartz photo-reactor for the measurement of the photocatalytic activity of the nanoparticles. To evaluate the degradation of RhB, the photo-reactor was irradiated with light from the solar simulator using a filter, with which the wavelengths shorter than 400 nm were cut off. Aliquots of the reaction mixture were collected and centrifuged at 15000 rpm for 10 min to separate the photocatalyst from the mixture, and UV-Vis-NIR absorption by the supernatant was recorded by the UV-Vis-NIR spectrophotometer for 90 min at regular intervals of time to measure the degradation of RhB. RhB molecules in aqueous solution show three major peaks at 258, 354 and 554 nm in the UV-Vis absorption spectrum. **Figure 6(a)** shows the time variations of the absorption spectrum in the presence of Ag@AgCl. The decrease in the peak intensity represents the degradation of RhB molecules, and there was no shift in the peak position, which elucidates that the degradation was induced by the destruction of benzene rings in RhB [23] [24]. The photocatalytic activity was evaluated by the UV-Vis absorption at 554 nm. The time variation of - ln (C/C_0), where C is the concentration of the dye at time t and C_0 the concentration at t = 0, is shown in **Figure 6(b)**. The rate constant k for the degradation reaction of RhB based on the first order reaction kinetics (ln (C/C_0) = - k t) is calculated to be 0.0186 min^{-1} and approximately 90 % of the RhB was degraded after 90 min. The high photocatalytic performance of Ag@AgCl NPs owes to the SPR of Ag NPs and the semiconductor features of AgCl NPs [25] [26]. It is clearly shown that the degradation of RhB was encouraged by the present Ag@AgCl NPs.
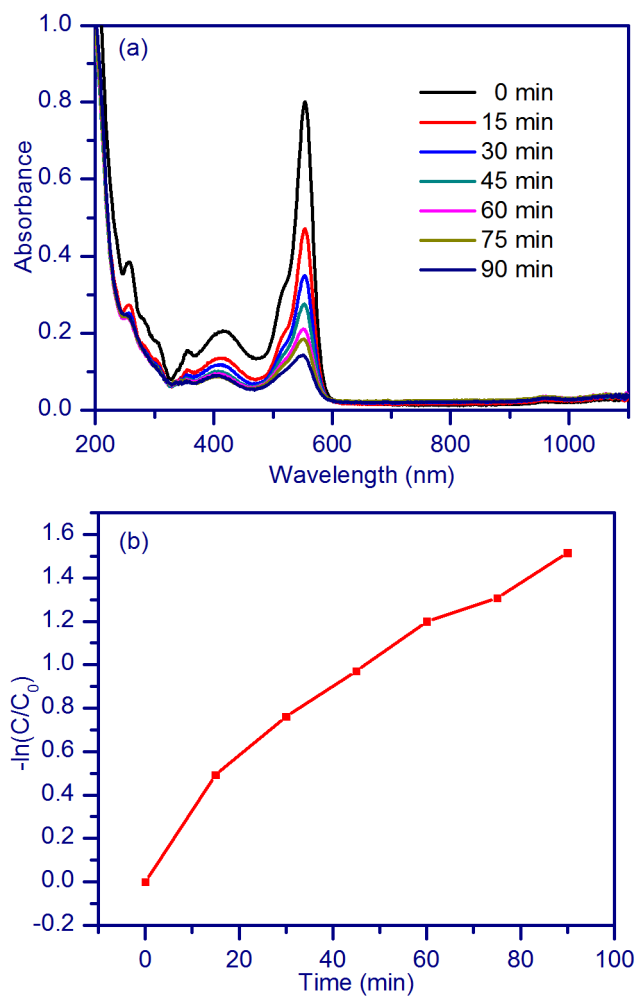
Figure 6. Degradation of RhB. (a) UV-Vis-NIR absorption spectrum of RhB degraded by Ag@AgCl NPs at regular intervals of time; (b) Time variation of –ln (C/C_0), where C is the concentration of the dye at time t and C_0 the concentration at t = 0 based on the peak at 554 nm.

Conclusion

4.5 Conclusions

A green method for synthesising an effective plasmonic photo catalyst was developed. An aqueous extract from needles of *Pinus densiflora* (red pine) was mixed with an aqueous solution of silver nitrate to synthesise silver nanoparticles (Ag NPs) and then clusters composed of silver and silver chloride particles (Ag@AgCl NPs) were synthesised exposing the Ag NPs to light from a solar simulator. The chlorine components present in the extract were utilised as a halide source. Ag NPs, which were formed in AgCl NPs via photo reduction, promoted the photocatalytic activity induced by surface plasmon resonance in visible light.

References

References

1. L. Han, P. Wang, C. Z. Zhu, Y. M. Zhai and S. J. Dong, *Nanoscale*, 2011, **3**, 2931-2935.

2. D. L. Chen, S. H. Yoo, Q. S. Huang, G. Ali and S. O. Cho, *Chemistry-a European Journal*, 2012, **18**, 5192-5200.

3. J. Tejeda, N. J. Shevchik, W. Braun, A. Goldmann and M. Cardona, *Physical Review B (Solid State)*, 1975, **12**, 1557-1566.

4. T. Hua and F. Wai Yip, *Chemical Physics Letters*, 2005, **406**, 289-293.

5. L. Ge, C. C. Han, J. Liu and Y. F. Li, *Applied Catalysis a-General*, 2011, **409**, 215-222.

6. C. C. Han, L. Ge, C. F. Chen, Y. J. Li, Z. Zhao, X. L. Xiao, Z. L. Li and J. L. Zhang, *Journal of Materials Chemistry A*, 2014, **2**, 12594-12600.

7. L. Xinhui, H. Jinlin, L. Jiajia, H. Yong, S. Yong, Y. Haijian, T. Guoxiu and Q. Haisheng, *Materials Letters*, 2013, **91**, 129-132.

8. J. Cao, B. D. Luo, H. L. Lin, B. Y. Xu and S. F. Chen, *Journal of Hazardous Materials*, 2012, **217**, 107-115.

9. D. Lihong, T. Shanshan, Z. Junyi, Z. Peiying, Z. Lifan and T. Fengwei, *Materials Letters*, 2013, **91**, 245-248.

10. Y. Yokouchi, Y. Ambe and K. Fuwa, *Chemosphere*, 1981, **10**, 209-213.

11. J.-I. Azuma, N. Takahashi and T. Koshijima, *Carbohydrate Research*, 1981, **93**, 94-104.

12. N. Y. Kim, M. K. Jang, D. G. Lee, K. H. Yu, H. Jang, M. Kim, S. G. Kim, B. H. Yoo and S. H. Lee, *Nutrition Research and Practice*, 2010, **4**, 16-22.

13. C. A. Rice-Evans, N. J. Miller and G. Paganga, *Free Radical Biology and Medicine*, 1996, **20**, 933-956.

14. J. Y. Song and B. S. Kim, *Bioprocess and Biosystems Engineering*, 2009, **32**, 79-84.

15. X. C. Ma, Y. Dai, L. Yu, Z. Z. Lou, B. B. Huang and M. H. Whangbo, *Journal of Physical Chemistry C*, 2014, **118**, 12133-12140.

16. G. Wang, T. Nishio, M. Sato, A. Ishikawa, K. Nambara, K. Nagakawa, Y. Matsuo, K. Niikura and K. Ijiro, *Chemical Communications*, 2011, **47**, 9426-9428.

17. M. M. Husein, E. Rodil and J. H. Vera, *Journal of Colloid and Interface Science*, 2005, **288**, 457-467.

18. P. Wang, B. B. Huang, X. Y. Qin, X. Y. Zhang, Y. Dai, J. Y. Wei and M. H. Whangbo, *Angewandte Chemie-International Edition*, 2008, **47**, 7931-7933.

19. J. G. McEvoy and Z. S. Zhang, *Applied Catalysis B-Environmental*, 2014, **160**, 267-278.

20. H. Lei, W. Ping, Z. Chengzhou, Z. Yueming and D. Shaojun, *Nanoscale*, 2011, **3**, 2931-2935.

21. H. Xu, H. M. Li, J. X. Xia, S. Yin, Z. J. Luo, L. Liu and L. Xu, *Acs Applied Materials & Interfaces*, 2011, **3**, 22-29.

22. C. D.Wagner, W. M. Riggs, L. E. Davis, J. F. Moulder and G. E. Muilenburg, *Handbook of X-ray Photoelectron Spectroscopy*, Perkin-Elmer Corp., Physical Electronics Division: Eden Prairie, Minnesota, 1979.

23. K. Yu, S. G. Yang, H. He, C. Sun, C. G. Gu and Y. M. Ju, *Journal of Physical Chemistry A*, 2009, **113**, 10024-10032.

24. S. N. Zhang, H. F. Tian, S. J. Zhang, L. M. Song, X. Q. Wu, J. Y. Ye and Q. W. Wei, *Chemical Engineering Journal*, 2014, **240**, 548-553.

25. Z. Y. Lin, J. Xiao, J. H. Yan, P. Liu, L. H. Li and G. W. Yang, *Journal of Materials Chemistry A*, 2015, **3**, 7649-7658.

26. R. F. Dong, B. Z. Tian, C. Y. Zeng, T. Y. Li, T. T. Wang and J. L. Zhang, *Journal of Physical Chemistry C*, 2013, **117**, 213-220.

Chapter 5

Conclusion

Conclusion

In chapter 2, silver nanoparticles (Ag NPs) were successfully synthesised by mixing a leaf extract from *Prunus yedoensis* with aqueous solution of AgNO$_3$. The particles showed their high dispersibility in water, biocompatibility, surface enhanced Raman scattering activity and antibacterial activity. We believe that the significant features possessed by the present Ag NPs were derived from the properties of both organic compounds capping the particles and core particles and therefore the Ag NPs may well be actively utilised in the field of biomedicine; e.g., as nano agents for bio-imaging, nano media for photothermal therapy, nano vehicles for drug delivery and detectors of biomolecules and biomaterials. It is also inferred from the previous and present studies that metal-filling organic compounds nanoparticles may commonly be synthesised via bio-reduction using plants' extracts. In chapter 3, a green method was developed for synthesizing silver with silver chloride nanoparticles (Ag@AgCl NPs), an effective plasmonic photocatalyst based on two-step procedure; i.e., (i) Production of AgCl NPs via the reduction of Ag+ (AgNO$_3$) using an aqueous leaf extract of *Solidago altissima,* and (ii) Production of Ag@AgCl NPs via the photo reduction of AgCl NPs. The optical properties and elemental compositions of as-synthesized Ag@AgCl NPs were well characterized. We found that degradation of RhB was effectively achieved thanks to both surface plasmon resonance and semiconductor properties of Ag@AgCl NPs. The particles also showed high surface-enhanced Raman scattering and anti-bacterial activities. The present green approach to the synthesis of nanoparticles using a weed may encourage the utilization of hazardous plants for the creation of novel nanomaterials. In chapter 4, a green method was developed for synthesizing silver with silver chloride nanoparticles (Ag@AgCl NPs), an effective plasmonic photocatalyst based on the methodology of chapter 3 using an aqueous leaf extract of *Pinus densiflora*.

The primary motive to use aqueous leaf extracts to synthesize novel nanomaterials was achieved. It is the fact that leaf extracts posses astonishing properties exclusively supreme medicinal properties in healing various diseases. In the published scientific literature it was reported that chemical

components of leaves have anti-cancerous properties and also various other properties. The nanoparticles synthesized by using plant leaf extract posses the properties of the leaf extract up to certain extent and can be used as a novel nanomedicine. Advancement in the nanotechnology made sufficiently possible in diagnosing various diseases at early stages of manifestation, however the permanent cure for various cancers and other diseases is not achieved. Based on the present research nanomedicines can be developed in a greener way with supreme properties. In additional, plant species are generally rich in certain elements, considering this various composite nanomaterials can be developed with hybrid properties.

Publications

1. Synthesis of nanoparticles composed of silver and silver chloride for a plasmonic photocatalyst using an extract from a weed *Solidago altissima* (goldenrod) Kumar V. A, Uchida T, Mizuki T, Nakajima Y, Katsube Y, Hanajiri T, Maekawa T. Advances in Natural Sciences: Nanoscience & Nanotechnology   7(1) 015002 (12 pp.)   2016

2. Synthesis of nanoparticles composed of silver and silver chloride for a plasmonic photocatalyst using an extract from needles of *Pinus densiflora*. Kumar V. A, Nakajima Y, Uchida T, Hanajiri T, Maekawa T. Materials Letters 176(1) 169 (4 pp.) 2016.